

# SpikACom: A Neuromorphic Computing Framework for Green Communications

Yanzhen Liu<sup>1</sup>, Zhijin Qin<sup>2\*</sup>, Yongxu Zhu<sup>3</sup>, Geoffrey Ye Li<sup>1</sup>

<sup>1</sup>Department of Electrical and Electronic Engineering, Imperial College  
London, SW7 2AZ, London, UK.

<sup>2\*</sup>Department of Electronic Engineering, Tsinghua University, 100084, Beijing,  
China.

<sup>3</sup>National Mobile Communications Research Laboratory, Southeast University,  
210096, Nanjing, China.

\*Corresponding author(s). E-mail(s): [qinzhijin@tsinghua.edu.cn](mailto:qinzhijin@tsinghua.edu.cn);  
Contributing authors: [yanzhen.liu22@ic.ac.uk](mailto:yanzhen.liu22@ic.ac.uk); [geoffrey.li@ic.ac.uk](mailto:geoffrey.li@ic.ac.uk);

## Abstract

The ever-growing power consumption of wireless communication systems necessitates more energy-efficient algorithms. This paper introduces SpikACom (**Spiking Adaptive Communication**), a neuromorphic computing-based framework for power-intensive wireless communication tasks. SpikACom leverages brain-inspired spiking neural networks (SNNs) for efficient signal processing. It is designed for dynamic wireless environments, helping to mitigate catastrophic forgetting and facilitate adaptation to new circumstances. Moreover, SpikACom is customizable, allowing flexibly integration of domain knowledge to enhance its interpretability and efficacy. We validate its performance on fundamental wireless communication tasks, including task-oriented semantic communication, multiple-input multiple-output (MIMO) beamforming, and orthogonal frequency-division multiplexing (OFDM) channel estimation. The simulation results show that SpikACom significantly reduces power consumption while matching or exceeding the performance of conventional algorithms. This study highlights the potential of SNNs for enabling greener and smarter wireless communication systems.

**Keywords:** neuromorphic computing, wireless communications, spiking neural network, continuous learning, energy-efficient, catastrophic forgetting

## 1 Introduction

Wireless communications have fundamentally changed the way people connect, communicate, and share information. However, the increasing power consumption of cellular systems also

raises public concerns on their environmental impact [1]. According to the Global enabling Sustainability Initiative (GeSI), the carbon emissions from the information and communications technology (ICT) sector in 2030 are expected to reach 1.25Gt  $CO_{2e}$  [2]. Moreover, by considering the enabling effect, 5G may potentially contribute to a reduction of 15% total global emissions [3, 4].

In wireless systems, the computational power is becoming increasingly dominant. A study by the University of Surrey shows that, in the massive multiple-input multiple-output (mMIMO) system, the computational power required for software-based signal processing is comparable to the energy consumption of radio frequency chains [5]. Moreover, with the development of AI-native wireless communications [6], computational energy consumption is expected to further increase, reaching a rate that far exceeds Moore’s Law [7]. Hence, an efficient computational architecture is critical for the sustainability of the ICT industry.

Spiking neural networks (SNNs) offer a promising solution to these challenges. Unlike traditional artificial neural networks (ANNs), SNNs more closely mimic the functioning of human brain. They emulate the electrical behaviour of biological neurons based on biophysical models and communicate through discrete events known as spikes. SNNs are characterized by high energy-efficiency, low latency, and sparsity [8], which is particularly appealing for wireless signal processing. Consequently, they have gained increasing research interest in recent years. Applications of SNNs in wireless communications include distributed neuromorphic edge computing [9], federated neuromorphic computing [10, 11], SNN-based semantic communication [12–14], and neuromorphic computing for physical layer signal processing [15–17]. However, these works are tailored for specific wireless tasks, limiting their general applicability. Moreover, they focus exclusively on the offline stage and are not adaptive to the changing wireless environments. A unified framework for designing and deploying SNNs in complex wireless environments is still lacking.

In this work, we propose a general framework for integrating SNNs into wireless communication systems, named SpikACom (**Spiking Adaptive Communication**). The framework is designed particularly for dynamic wireless environments, enabling quick adaptation to new channel distributions while simultaneously alleviating catastrophic forgetting. This allows the SNN to evolve over time and become increasingly powerful. Moreover, SpikACom requires few historical channel samples and has low computational complexity, making it suitable for resource-limited edge computing. The framework is also flexible and easy to incorporate domain knowledge into the design, thereby simultaneously achieving high energy efficiency and superior performance. To validate its effectiveness, we apply SpikACom to three representative wireless communication tasks: task-oriented semantic communication,

multiple-input multiple-output (MIMO) beamforming, and orthogonal frequency-division multiplexing (OFDM) channel estimation. From simulation results, SpikACom enables quick adaptation without catastrophic forgetting. Additionally, SNNs consume significantly less energy than conventional ANNs and traditional model-based methods while achieving comparable or even superior performance. Our study showcases the power of neuromorphic computing in developing more sustainable, intelligent, and powerful wireless communication systems.

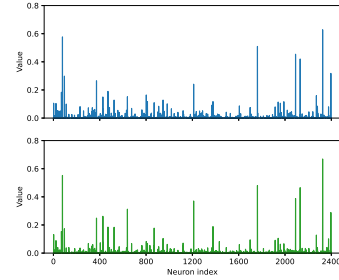
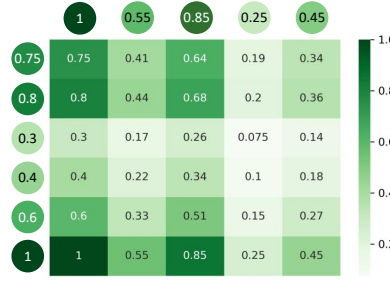
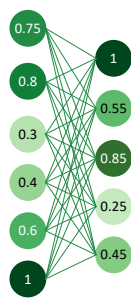
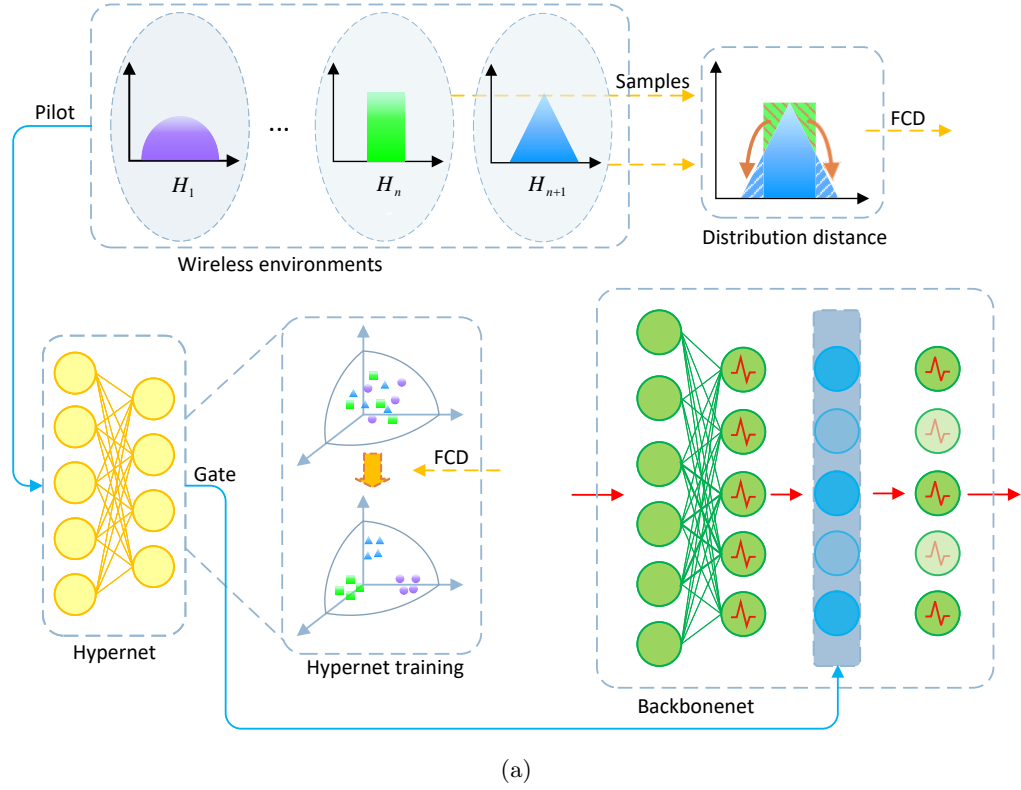
## 2 Results

### 2.1 Neuromorphic Continuous Learning Framework

In wireless communications, electromagnetic signals propagate through complex environments. Various factors, such as mobility, obstacles, weather conditions, and interference, can cause shifts in channel distributions and deteriorate the performance of offline-trained models. Consequently, deep learning models in wireless environments must be able to detect changes in channel distributions and quickly adapt to new circumstances. Moreover, due to limited memory budgets, these models have restricted access to previous channel state information (CSI) and are primarily updated based on current channel samples. This paradigm is known as continuous learning or lifelong learning in the field of machine learning [18].

A critical challenge in continuous learning is catastrophic forgetting, where acquiring new information leads to the loss of previously learned knowledge. Catastrophic forgetting hinders the model’s ability to self-evolve and reduce efficiency, as the model must constantly update itself, even when encountering an environment it has previously learned. In this work, we propose a general framework for deploying SNN in wireless communication systems, which efficiently mitigates the problem of catastrophic forgetting while maintaining low computational and memory cost.

Fig. 1 illustrates the proposed SpikACom, which is structured as a two-level control system. The first level provides coarse control at the neuron level while the second level offers finer control at the synaptic weights level. As shown in Fig. 1a, the first level control employs a hypernet to continuously explore the relationship between different channel distributions and uses its output signals to regulate the backbone SNN. The hypernet functions as a mapping, which transforms the high-dimensional probability space of the channel distributions into a low-dimensional vector while preserving their relative distance. This enables the separation of learning parameters for distinct environments, thereby reducing interference and alleviating catastrophic forgetting. Additionally, it facilitates significant parameter



(b)

(c)

**Fig. 1: Proposed SpikACom: A neuromorphic continuous learning framework for wireless communications.** (a) Neuron-level control: a hypernet which continuously reveals the relationships between different channel distributions and uses its output gate to control the spiking neurons of the backbone network. (b) Synaptic weight-level control: the proposed low-complexity SRC for regularizing synaptic weights. Left: spiking neurons and their associated spiking rates. Right: the regularization matrix for synaptic weights, which is defined as the outer product of two adjacent spiking rate vectors. (c) Comparison between SRC and EWC on task-oriented semantic communication experiment. Top: spiking rate vector. Bottom: singular vector corresponding to the largest singular value of the FIM.

reuse in similar environments and helps improve learning efficiency. To quantify the distance between different channel distributions, we propose a new metric, called Fréchet Channel Distance (FCD) (see Method), allowing for effective and versatile evaluation of the relationship between different wireless environments.

The second level provides finer control by regulating synaptic weights through a mechanism, called spiking rate consolidation (SRC), which uses the activity level of spiking neurons to denote the importance of synaptic weights, as illustrated in Fig. 1b. The motivation behind SRC is straightforward: active neurons carry more information and should be regulated with stronger weights, whereas inactive neurons are less important for the current task and removing them could have negligible impact [19]. Compared to the classic regularization-based method, elastic weight consolidation (EWC) [20], which uses the Fisher information matrix (FIM) to represent the importance of synaptic weights, SRC has much lower computational complexity and memory cost. However, SRC is effective and can achieve performance close to EWC. Fig. 1c compares the spiking rate vector with the eigenvector corresponding to the largest singular value of the FIM. From the figure, they closely resemble each other, suggesting that SRC captures the principal components of important synaptic weights.

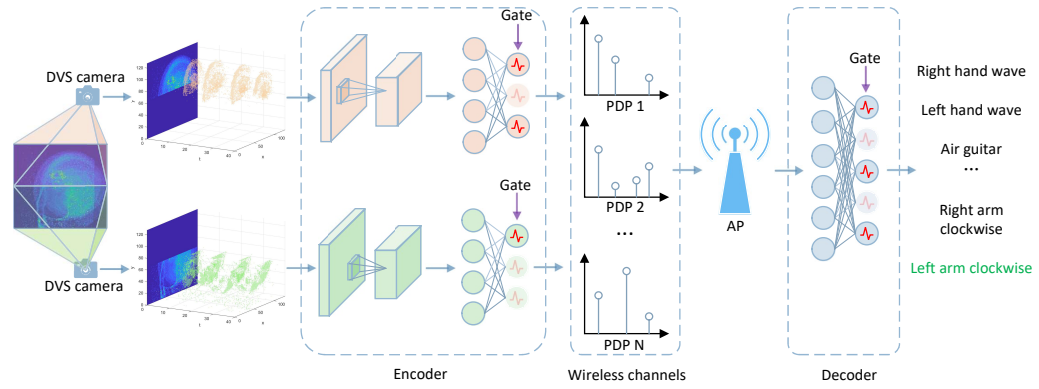
## 2.2 Task-oriented Semantic Communication

Semantic communication is seen as a revolutionary technology for 6G and beyond [21]. Instead of communicating at the bit level, semantic communication transmits task-related semantics, thereby boosting communication efficiency [22, 23]. However, extracting high-level semantics can be computationally intensive, which is impractical for resource limited edge devices. Therefore, we use SNNs as the backbone for semantic communication systems. Specifically, we consider a distributed remote inference task, as illustrated in Fig. 2a. Multiple distributed sensors collect signals from the physical world and encode them using SNNs. The encoded spikes are then transmitted to an access point (AP) through wireless channels. Upon receiving the signals, the AP feeds them into the SNN decoder and obtains the classification result. We adopt the DVS128 Gesture recognition task [24] as the testbed. Moreover, the proposed SpikACom is employed to mitigate catastrophic forgetting and enhance the adaptability of SNNs to fast-varying channels.

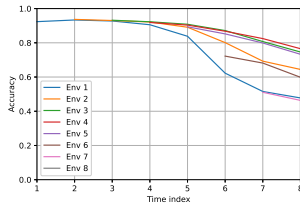
Fig. 2b-Fig. 2d illustrate the performance trajectory of analysed schemes<sup>1</sup>. The vanilla fine-tuning method (Fig. 2b) fails to address catastrophic forgetting, resulting in significant

---

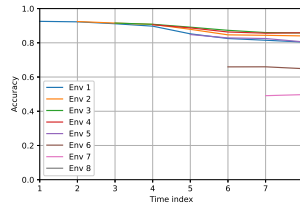
<sup>1</sup>We arrange the environments in descending order of SNR for better visualization. Hence, environments that appear later exhibit lower accuracy. However, our method is robust to permutations and interested readers can refer to the Supplementary for further details.



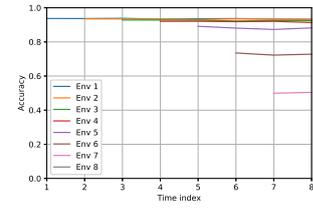
(a)



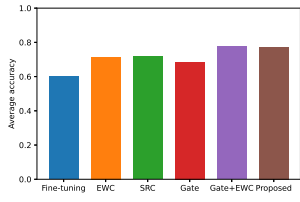
(b)



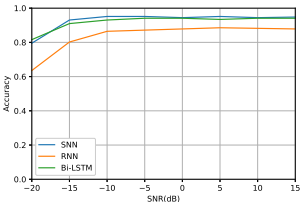
(c)



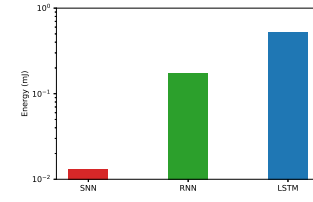
(d)



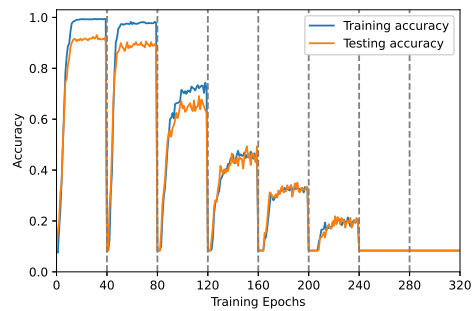
(e)



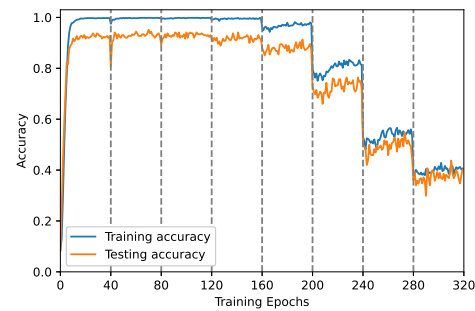
(f)



(g)



(h)



(i)

**Fig. 2: Performance of proposed SpikACom on task-oriented semantic communication.** (a) System model of the task-oriented semantic communication. (b)-(d) Learning trajectories of vanilla fine-tuning, EWC, and the proposed method. (e) Ablation study of the proposed algorithm. We show the average accuracy in the last environment. (f) Performance comparison of SNN vs RNN and Bi-LSTM. (g) Energy comparison of SNN vs RNN and Bi-LSTM. (h)-(i) Convergence curves of the orthogonal gate and hypernet gate.

drop in inference accuracy over time. The EWC method (Fig. 2c) helps alleviate this performance degradation to some extent, but accuracy still declines as the channel distribution shifts. As shown, accuracy under the initial channel environment decreases by approximately 10% after the network experiences 8 different environments. Additionally, EWC imposes increasingly strong constraints on the parameter space as the network learns more environments, leading to lower inference accuracy in later stages (Environment 6). In contrast, our proposed method (Fig. 2d) not only prevents catastrophic forgetting but also maintains high accuracy in new environments. This is because SpikACom effectively leverages the relationship between different channel distributions, providing more efficient management of plasticity while ensuring stability.

Fig. 2e shows the ablation study of our proposed algorithm. The baseline fine-tuning method achieves an average accuracy of only 60.15%. The EWC regularization helps alleviate catastrophic forgetting and improves accuracy to 71.54%. Our proposed SRC regularization method achieves 71.64% accuracy, which is very close to that of EWC. This demonstrates that SRC is as effective as the EWC in accessing the importance of synaptic weights. However, SRC has significantly lower computational cost and memory requirements compared to EWC, which is more suitable for wireless communication scenarios. Additionally, incorporating a hypernet gate alone increases the average accuracy to 68.42%. Combining the hypernet gate with EWC yields strong performance, with an average accuracy of 77.47%. Similarly, the combination of hypernet gate with SRC achieves an average accuracy of 77.42%, indicating that it effectively mitigates catastrophic forgetting.

Fig. 2f compares SNN with conventional ANN architectures, including recurrent neural network (RNN) and bi-directional long short-term memory (Bi-LSTM) [25, 26]. The results show that SNN achieve comparable or even superior performance to Bi-LSTM and perform significantly better than RNN, across different signal-to-noise ratio (SNR) values. In terms of energy consumption (Fig. 2g), SNN consumes approximately an order of magnitude less energy compared to Bi-LSTM and RNN. These results indicate that SNN is highly efficient for semantic communications, providing satisfactory performance while significantly improving energy efficiency.

Fig. 2h-Fig. 2i compare our proposed algorithm with a trivial orthogonal gate method. The orthogonal gate approach divides neurons into uniformly disjoint groups, assigning each environment a distinct group of neurons for training. While this method avoids catastrophic forgetting, it is inefficient due to the limited number of neurons assigned to each environment, resulting in insufficient plasticity. Furthermore, previously learned knowledge does not aid the network in adapting to current channel distributions. As a result, the network must

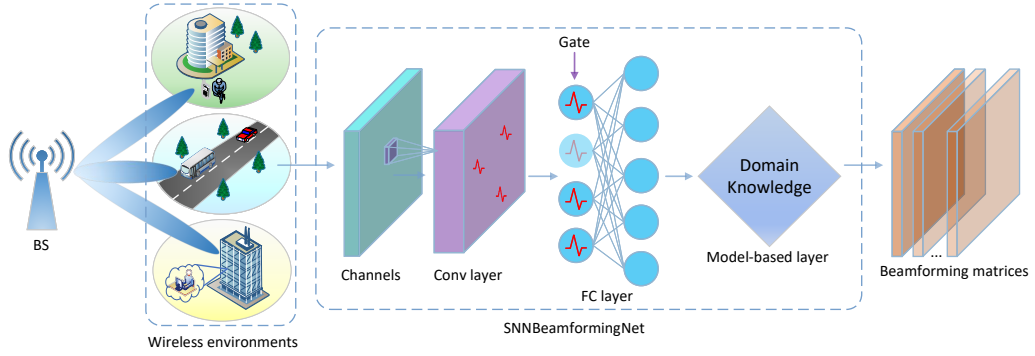
relearn from scratch when a new environment comes, leading to long convergence time and suboptimal performance. As shown in Fig. 2h, the orthogonal gate method performs poorly in later environments and even fails to converge when the SNR is very low (epochs 240 - 320). In contrast, our proposed framework efficiently leverages the correlation between different environments, allowing the SNNs to start from a favourable initial point. Hence, as observed in Fig. 2i, our method adapts to new environments significantly faster and achieves superior performance.

### 2.3 MIMO Beamforming

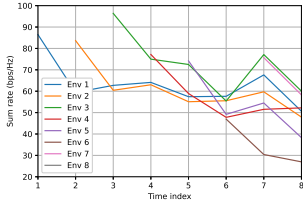
Beamforming is a key signal processing technique in MIMO systems [27]. It allows a transmitter to shape and focus its signal toward a target receiver by adjusting the amplitude and phase of the signal at each antenna, therefore increasing signal strength at the intended receiver while minimizing interference to other users. In recent years, deep learning techniques have been applied to optimize beamforming [28–31], leveraging neural networks to improve performance and reduce complexity. However, conventional ANNs still involve large-scale matrix-vector multiplications, which is energy-demanding. Moreover, there lacks an efficient method to deploy such deep-learning based beamforming algorithms in dynamic wireless environments. Therefore, as illustrated in Fig. 3a, we employ the proposed SpikA-Com framework for beamforming. It is important to note that, to improve the performance and interpretability of SNN-based beamforming, we incorporate domain knowledge into the design of the backbone SNNBeamformingNet (see Method), making it not merely a black-box architecture.

We first investigate the performance of our proposed framework in combating catastrophic forgetting. From Fig. 3b, the sum rate of the vanilla fine-tuning method drops sharply. This is different from the semantic communication task, where accuracy declines smoothly. The difference is due to two main reasons. First, environments are set more distinctly in beamforming than in semantic communication tasks. Second, the design of beamforming involves complex, large-scale optimization, where outputs are highly sensitive to inputs. As a result, shifts in distribution significantly impact performance. Fig. 3c shows the performance of EWC in combating catastrophic forgetting. While EWC mitigates the performance drop to some extent, accuracy still decreases as distributions change. Our proposed method (Fig. 3d), however, efficiently addresses catastrophic forgetting, without evident performance drop as the network learns across multiple environments.

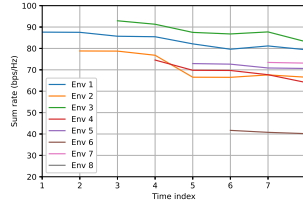
Fig. 3e presents an ablation study on the beamforming tasks. The results show that the average sum rate of fine-tuning is 52.68 bps/Hz. The EWC method improves this average



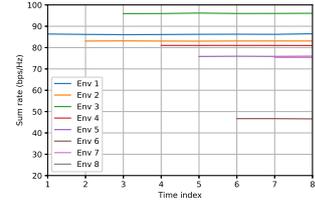
(a)



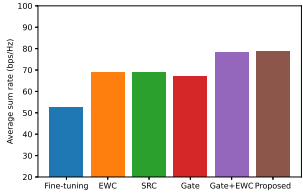
(b)



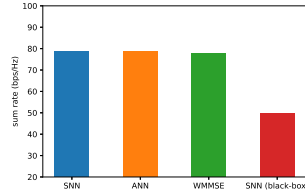
(c)



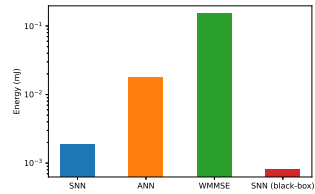
(d)



(e)



(f)



(g)

**Fig. 3: Performance of proposed SpikACom for MIMO beamforming.** (a) System model of the SNN-based MIMO beamforming. (b)-(d) Learning trajectory of vanilla fine-tuning, EWC, and proposed method. (e) Ablation study of proposed algorithm. We show the average sum rate at the last environment. (f) Performance comparison of SNN-based beamforming vs ANN-based beamforming, black-box SNN, and WMMSE. (g) Energy comparison between SNN, ANN, black-box SNN, and WMMSE.

rate to 69.13 bps/Hz, which alleviates catastrophic forgetting to a certain extent. Additionally, our proposed SRC regularization method also achieves comparable performance to EWC, at 68.87 bps/Hz. Hypernet gate alone gives an performance of 66.90 bps/Hz, which is slightly worse than purely regularization based methods. The combination of the hypernet gate method with synaptic weights regularization achieves the best performance, yielding

an average sum rate of 78.43 bps/Hz and 78.67 bps/Hz for gate+EWC and gate+SRC, respectively.

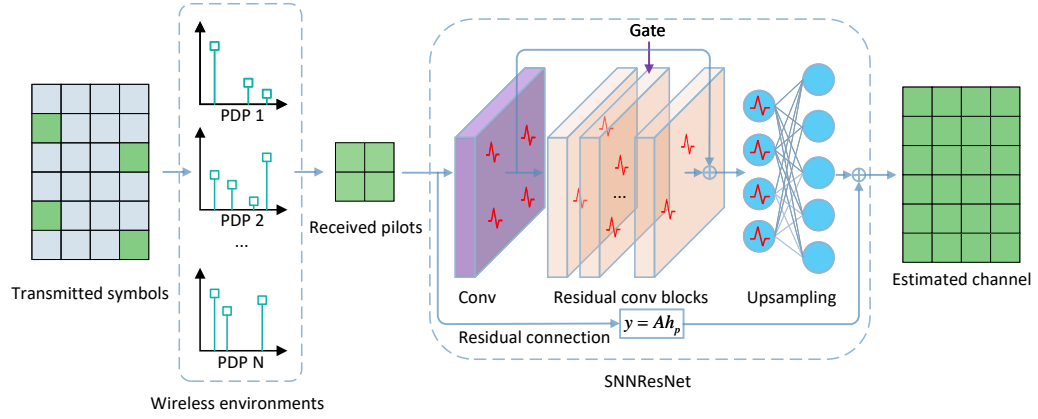
Fig. 3f compares SNN-based beamforming with ANN-based beamforming, the traditional optimization-based method weighted minimum mean-squared error (WMMSE), and black-box SNN (i.e., SNN without the model-driven layer). From the figure, the average sum-rate of SNN-based beamforming is 78.65 bps/Hz, closely matching 78.78 bps/Hz achieved by ANN-based beamforming. Notably, the average sum rate of WMMSE is slightly lower at 77.85 bps/Hz. This is due to WMMSE use block coordinate descent for optimization, which can easily become trapped in local optima, especially under complex and unbalanced channel conditions. In contrast, deep-learning-based methods excel in such scenarios and achieve superior performance. The black-box SNN performs poorly, with an average sum-rate of only 49.94 bps/Hz, which highlights the significant performance improvement brought by incorporating domain knowledge into deep-learning modules.

Regarding energy consumption (Fig. 3g), SNN-based beamforming consumes only 0.002 mJ per optimization, which is significantly lower than the 0.018 mJ required for ANN-based beamforming and the 0.16 mJ for the WMMSE algorithm. The black-box SNN achieves the lowest energy consumption at just 0.00082 mJ owing to its purely SNN-based architecture. However, considering the performance trade-off, incorporating the model-driven layer remains critical for MIMO beamforming.

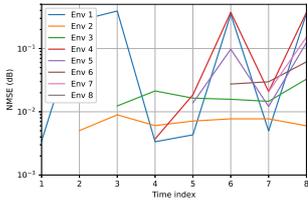
## 2.4 OFDM Channel Estimation

OFDM is known for its high spectral efficiency and resilience to multipath fading, which is a foundational technology in wireless communication [32, 33]. To maximize throughput in OFDM systems, obtaining accurate channel information is crucial. Recent years have witnessed the rapid development of deep learning-based channel estimation algorithms, which have achieved empirical success compared to traditional channel estimation methods [34, 35]. However, the high energy consumption of these deep-learning models hinders their practical deployment. Therefore, in this work, we develop SNN-based OFDM channel estimation algorithms based on the proposed SpikACom for improved efficiency.

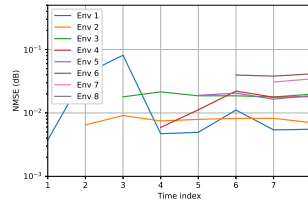
Fig. 4b-Fig. 4d show the performance trajectory of the compared schemes. Specifically, we use the WINNER channel as the testbed, which includes diverse propagation environments with distinct characteristics, such as environment 1 (indoor small office) and environment 3 (bad urban micro-cell), as well as similar environments, like environment 1 and environment 4 (urban macro-cell). In Fig. 4b, the vanilla fine-tuning method exhibits noticeable fluctuations in performance due to significant variations in the channel distribution. This method



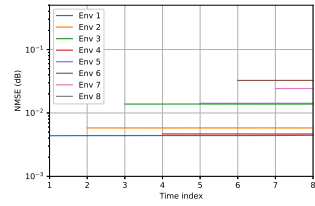
(a)



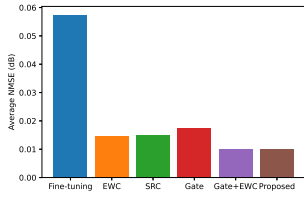
(b)



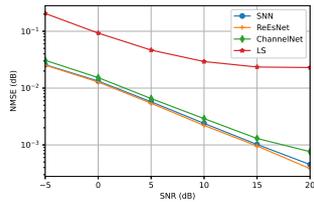
(c)



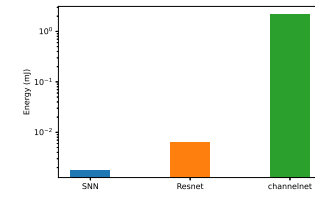
(d)



(e)



(f)



(g)

**Fig. 4: Performance of proposed SpikACom for OFDM channel estimation. (a)** System model of the SNN-based OFDM channel estimation. **(b)-(d)** Learning trajectory of vanilla fine-tuning, EWC, and proposed method. **(e)** Ablation study of proposed algorithm. We show the logarithm average of NMSE at the last environment. **(f)** Performance comparison of SNN vs LS, ReEsNet, and ChannelNet. **(g)** Energy comparison between SNN, ReEsNet, and ChannelNet.

trains the model on a new environment without preserving past knowledge. Consequently, its performance in earlier environments depends solely on how similar the new environment is to the previous ones. If the new environment differs significantly, the model performs poorly in previous environments, resulting in unstable performance. The EWC method (Fig. 4c) mitigates this degradation to some extent by preserving some learned knowledge. However,

it fails to explore the relationships between past knowledge and the current environment, leading to significant performance drops when the distributional distance is large (as shown by the high NMSE of environment 1 at time index 3). In contrast, our proposed method (Fig. 4d) effectively leverages the relationship between past and new environments, using this information to guide the backbone network to learn in a more intelligent and efficient manner, which stabilizes performance across different environments.

Fig. 4e presents the ablation study of our proposed algorithm. The performance of fine-tuning is poor, achieving an average normalized mean-squared error (NMSE) of only 0.056 dB. Both the EWC regularization and our proposed SRC method achieve similar performance, with NMSEs of 0.0148 dB and 0.0150 dB, respectively. The hypernet method also helps alleviate catastrophic forgetting, achieving an NMSE of 0.0176 dB. Combining these two-level controls yields the best performance, reducing the NMSE to 0.0099 dB.

Fig. 4f compares SNN with conventional least-square (LS) estimator and two representative ANN-based OFDM channel estimation methods, namely ChannelNet [34] and ReEsNet [35]. ChannelNet decomposes channel estimation into a super-resolution module and a denoising module. In contrast, ReEsNet enables end-to-end channel estimation and utilizes residual blocks to enhance performance, which is regarded as one of the most efficient ANN architectures for OFDM channel estimation. From Fig. 4f, the performance of LS is very poor and falls far behind deep learning-based methods. ReEsNet achieves the lowest NMSE, but the performance of SNN is very close and better than ChannelNet. This demonstrates that SNN, despite relying on sparse spikes for computation, can effectively handle the complex task of OFDM channel estimation and achieve performance on par with floating-point operations-based ANN architectures.

In terms of energy consumption (Fig. 4g), SNN requires only 0.0018 mJ per estimation, which is approximately 3.5 times more energy-efficient than 0.0064 mJ consumed by ReEsNet. The ChannelNet, however, is very energy-intensive and consumes 2.19 mJ per estimation due to its large network size. These results underscore the high efficiency of SNN for OFDM channel estimation.

## 3 Methods

### 3.1 Spiking Neuron Model

In this work, we assume the widely used leaky integrate-and-fire (LIF) neuron model. The dynamics of a LIF neuron can be formulated as

$$\bar{V}[t] = V[t-1] + \frac{1}{\tau}(V[t-1] - V_{\text{reset}}) + X[t], \quad (1)$$

$$S[t] = \Theta(\bar{V}[t] - V_{\text{th}}), \quad (2)$$

$$V[t] = (1 - S[t])\bar{V}[t] + S[t]V_{\text{reset}}, \quad (3)$$

where  $\bar{V}[t]$  represents the membrane potential of the spiking neuron at time step  $t$ , and  $\tau$  is a constant that defines the leaky rate.  $V_{\text{reset}}$  denotes the reset membrane potential, and  $X[t]$  is the input current. When the membrane potential reaches threshold  $V_{\text{th}}$ , a spike is generated, denoted by  $S[t] \in \{0, 1\}$ . Function  $\Theta(\cdot)$  is the Heaviside step function. Equation (3) indicates that membrane potential  $V[t]$  will be reset to  $V_{\text{reset}}$  when a spike is triggered.

We train the SNNs using the SpikingJelly framework [36]. All SNNs are trained using back propagation through time (BPTT) with the surrogate gradient method [37]. Unless stated otherwise, we use a batch size of 64 and a learning rate of  $1 \times 10^{-3}$ . The Adam optimizer is employed and a cosine annealing schedule is used to adjust the learning rate.

### 3.2 Hypernet

The hypernet exploits the relationships between different wireless environments and extracts distribution-related information to guide the backbone network. By doing so, previously learned knowledge can be utilized to accelerate adaptation in similar environments. While for differing channel distributions, the synaptic weights of the backbone network are separated to avoid catastrophic forgetting. This method is primarily inspired by the hybrid modulation network (HMN) [38], but we introduce several key improvements. First, whereas HMN uses a gate to modulate the firing threshold of spiking neurons, we find that using a binary gate to control the on/off states of spiking neurons is more effective [39]. Second, HMN is developed exclusively for the permuted MNIST dataset, which restricts its applicability to other continuous learning scenarios. In this work, we propose computing the distance between different distributions using a general metric, making our approach not only more effective but also applicable to a broad range of tasks. Furthermore, we derive generalization bounds to provide a theoretical foundation for our method (see Supplementary).

### 3.2.1 Metric for Channel Distribution Distance

Quantifying the distance between different environments is crucial for our method. There are several widely used metrics for measuring the distribution distance, including f-divergence, total variation distance, and earth mover’s distance (EMD). In this paper, we adopt EMD due to its good continuity, which helps stabilize neural network training [40]. Specifically, EMD is defined as the minimal cost for transforming one distribution into another:

$$\text{EMD}(Q, P) = \inf_{\gamma \in \Gamma(Q, P)} \int_{X \times Y} d(x, y) d\gamma(x, y), \quad (4)$$

where  $\Gamma(Q, P)$  denotes the set of all joint distributions whose marginals are  $Q$  and  $P$ ,  $d(x, y)$  represents a distance measure, which by default is the  $L_2$  norm. However, computing the EMD distance involves solving a complex optimization problem, which incurs significant computational burden. To address this issue, we propose FCD inspired by the Fréchet Inception Distance (FID) [41]. Specifically, for two Gaussian distributions  $\mathcal{N}(\mu_1, \Sigma_1)$  and  $\mathcal{N}(\mu_2, \Sigma_2)$ , their EMD can be computed in closed form as:

$$\text{EMD}(\mathcal{N}(\mu_1, \Sigma_1), \mathcal{N}(\mu_2, \Sigma_2)) = \|\mu_1 - \mu_2\|_2^2 + \text{Tr}(\Sigma_1 + \Sigma_2 - 2(\Sigma_1 \Sigma_2)^{\frac{1}{2}}). \quad (5)$$

Given two channel distributions  $\mathcal{H}_1$  and  $\mathcal{H}_2$ , we map the samples to a new space through a function  $f$  and fit two Gaussian distributions for  $f(\mathcal{H}_1)$  and  $f(\mathcal{H}_2)$ , respectively. Then, the FCD is obtained by substituting the fitted parameters into equation (5). In short, the FCD is formally defined as

$$\text{FCD}(\mathcal{H}_1, \mathcal{H}_2) \triangleq \|\mu_1 - \mu_2\|_2^2 + \text{Tr}(\Sigma_1 + \Sigma_2 - 2(\Sigma_1 \Sigma_2)^{\frac{1}{2}}), \quad (6)$$

where  $\mu_1 = \mathbb{E}_{h_1 \sim \mathcal{H}_1}[f(h_1)]$ ,  $\mu_2 = \mathbb{E}_{h_2 \sim \mathcal{H}_2}[f(h_2)]$ ,  $\Sigma_1 = \text{cov}_{h_1, h'_1 \sim \mathcal{H}_1}(f(h_1), f(h'_1))$ , and  $\Sigma_2 = \text{cov}_{h_2, h'_2 \sim \mathcal{H}_2}(f(h_2), f(h'_2))$ . Notably, we employ the encoder from CSI-net [42] as function  $f$  because CSI-net is specifically designed for CSI compression, making it more suitable for wireless communication tasks compared to the Inception network [43] that is trained on natural images.

It is worth mentioning that based on some assumptions of the underlying physical channel models, we can derive concise expression for the EMD. Furthermore, the inherent domain knowledge also provides a solid foundation for the hypernet to generalize across different channel distributions. Please refer to the Supplementary for details.

### 3.2.2 Hypernet Training Loss

We train the hypernet so that its output gate can represent the relationship between different environments. To this end, we employ the cosine distance as the loss function for training the hypernet. Specifically, given input samples  $h_1 \sim \mathcal{H}_1$  and  $h_2 \sim \mathcal{H}_2$ , denoting the output gates as  $\mathbf{g}_1$  and  $\mathbf{g}_2$ , the loss function is defined as follows:

$$\mathcal{L}_h(h_1, h_2) \triangleq \left( \frac{\mathbf{g}_1^T \mathbf{g}_2}{\|\mathbf{g}_1\| \|\mathbf{g}_2\|} - \exp(-\gamma \text{FCD}(\mathcal{H}_1, \mathcal{H}_2)) \right)^2 + \lambda \sum_{i=1,2} (\|\mathbf{g}_i\|_1 - \rho)^2, \quad (7)$$

where the exponential function is used to normalize the FCD to  $[0, 1]$ , the last term controls the sparsity of the output gate, and  $\gamma$ ,  $\lambda$ , and  $\rho$  are constants that should be carefully chosen.

### 3.3 Semantic Communication

We consider a multi-user semantic communication system with  $I = 2$  distributed sensors and evaluate our algorithms on the DVS128 Gesture dataset [24]. Specifically, the gesture samples are uniformly divided into  $I$  segments and then fed into the corresponding semantic encoder of the  $i$ th sensor. Each semantic encoder consists of 5 stacked SNN blocks [44], comprising a 2D convolutional layer with *output channel* = 64, *kernel size* =  $3 \times 3$ , and *stride* = 1; a batch normalization layer; a LIF neuron layer; and a max pooling layer with *kernel size* = 2 and *stride* = 2. Each channel encoder consists of two spiking fully connected (FC) layers with 3,200 and 512 spiking neurons, respectively. The spikes output by the channel encoder are then reshaped into complex numbers for transmission, with a block length of 256. The simulation time step is set as  $T = 16$  and we assume the channel coherence time equals the transmission time of a single block of data. Moreover, since we focus on varying channels, the semantic encoders are trained under lossless channels and remain fixed during subsequent tests. Only the channel encoder and channel decoder are updated when the channel PDPs change.

Regarding the wireless channels, we adopt a multipath channel model with  $L = 8$  taps [45]. Denoting the transmitted signal as  $x$ , the received signal  $y$  can be written as

$$y = x * h + n, \quad (8)$$

where  $h$  denotes the instantaneous channel and  $n \sim \mathcal{N}(0, \sigma^2)$  is the additive white Gaussian noise (AWGN). The SNR is defined as

$$\text{snr} \triangleq \frac{E(|x * h|^2)}{E(n^2)} = \frac{\sum_{l=1}^L E(|h_l|^2) E(|x|^2)}{\sigma^2}. \quad (9)$$

We fix  $E(|x|^2)/\sigma^2$  at 0 dB, and set the channel gain  $\sum_{l=1}^L E(|h_l|^2)$  within the range of 0 to  $-28$  dB with a uniform interval of 4 dB. The channel decoder consists of a 1D spiking convolutional layer with *output channel* = 16, *kernel size* = 13, and *stride* = 1; two FC layers with spiking neuron counts of 3,200 and 110, respectively; and a voting layer with a dimension of 10 [44].

### 3.4 MIMO Beamforming

We consider a downlink MIMO system with a single base station (BS) serving  $K$  users simultaneously. Since the core function of beamforming is to boost the system throughput, we consider the following sum rate maximization problem:

$$\max_{\mathbf{V}_k} \sum_{k=1}^K \alpha_k R_k, \quad (10a)$$

$$s.t. \sum_{k=1}^K \text{Tr}(\mathbf{V}_k \mathbf{V}_k^H) \leq P_T, \quad (10b)$$

where  $\mathbf{V}_k \in \mathbb{C}^{N_t \times d}$  is the beamforming matrix for user  $k$ , with  $N_t$  and  $d$  denoting the number of transmitting antennas and data streams, respectively<sup>2</sup>,  $\alpha_k$  and  $P_T$  denote the weight of user  $k$  and the total transmitting power, respectively.  $R_k$  denotes the theoretically achievable rate<sup>3</sup> and its expression is given by

$$R_k = \log \det \left( \mathbf{I} + \mathbf{H}_k \mathbf{V}_k \mathbf{V}_k^H \mathbf{H}_k^H \left( \sum_{l \neq k} \mathbf{H}_l \mathbf{V}_l \mathbf{V}_l^H \mathbf{H}_l^H + \sigma_k^2 \mathbf{I} \right)^{-1} \right), \quad (11)$$

where  $H_k \in \mathbb{C}^{N_r \times N_t}$  represents the channel between the BS and user  $k$ , and  $\sigma_k^2$  denotes the noise power of user  $k$ .

#### 3.4.1 WMMSE

Problem (10) is challenging to solve due to the highly-coupled non-convex rate expression (11). To tackle this issue, the WMMSE [46] algorithm equivalently reformulates problem (10) into the following more tractable form

$$\min_{\mathbf{W}_k, \mathbf{U}_k, \mathbf{V}_k} \sum_{k=1}^K \alpha_k (\text{Tr}(\mathbf{W}_k \mathbf{E}_k) - \log \det(\mathbf{W}_k)) \quad (12a)$$

<sup>2</sup>For simplicity, we assume that all users require the same number of data streams  $d$  and have the same number of receiving antennas  $N_r$ .

<sup>3</sup>In this work, we assume linear precoding.

$$\text{s.t. } \sum_{k=1}^K \text{Tr}(\mathbf{V}_k \mathbf{V}_k^H) \leq P_T, \quad (12b)$$

where  $\mathbf{W}_k \in \mathbb{C}^{d \times d}$  is an auxiliary weight matrix for user  $k$  and

$$\mathbf{E}_k \triangleq (\mathbf{I} - \mathbf{U}_k^H \mathbf{H}_k \mathbf{V}_k)(\mathbf{I} - \mathbf{U}_k^H \mathbf{H}_k \mathbf{V}_k)^H + \sum_{l \neq k} \mathbf{U}_k^H \mathbf{H}_k \mathbf{V}_l \mathbf{V}_l^H \mathbf{H}_k^H \mathbf{U}_k + \sigma_k^2 \mathbf{U}_k^H \mathbf{U}_k \quad (13)$$

with  $\mathbf{U}_k \in \mathbb{C}^{N_r \times d}$  being a virtual receive beamforming matrix for user  $k$ .

Problem (12) can be solved using the block coordinate descent algorithm. Specifically, variables  $\mathbf{W}_k, \mathbf{U}_k, \mathbf{V}_k$  are optimized in turn, with their optimal solutions given by

$$\mathbf{U}_k = \mathbf{A}_k^{-1} \mathbf{H}_k \mathbf{V}_k, \quad (14)$$

$$\mathbf{W}_k = \mathbf{E}_k^{-1}, \quad (15)$$

$$\mathbf{V}_k = \alpha_k \mathbf{B}^{-1} \mathbf{H}_k^H \mathbf{U}_k \mathbf{W}_k, \quad (16)$$

respectively, where

$$\mathbf{A}_k = \frac{\sigma_k^2}{P_T} \sum_{k=1}^K \text{Tr}(\mathbf{V}_k \mathbf{V}_k^H) \mathbf{I} + \sum_{l=1}^K \mathbf{H}_k \mathbf{V}_l \mathbf{V}_l^H \mathbf{H}_k^H, \quad (17)$$

$$\mathbf{E}_k = \mathbf{I} - \mathbf{U}_k^H \mathbf{H}_k \mathbf{V}_k, \quad (18)$$

and

$$\mathbf{B} = \sum_{k=1}^K \frac{\sigma_k^2}{P_T} \text{Tr}(\alpha_k \mathbf{U}_k \mathbf{W}_k \mathbf{U}_k^H) \mathbf{I} + \sum_{l=1}^K \alpha_l \mathbf{H}_l^H \mathbf{U}_l \mathbf{W}_l \mathbf{U}_l^H \mathbf{H}_l. \quad (19)$$

### 3.4.2 Model-based Layer

The goal of beamforming is to design beamforming matrices  $\mathbf{V}_k$ . However, directly setting the network output to  $\mathbf{V}_k$  results in poor performance because such a purely black-box structure cannot effectively handle the sophisticated beamforming optimization. To address this, we draw inspiration from the WMMSE algorithm and incorporate domain knowledge into the design of SNN-based beamforming. By reviewing subsection 3.4.1, we observe that the core aspect of the WMMSE algorithm is the introduction of auxiliary variables  $\mathbf{W}_k$  and  $\mathbf{U}_k$ . Therefore, we let the network output be  $\mathbf{W}_k$  and  $\mathbf{U}_k$ , and compute  $\mathbf{V}_k$  by substituting  $\mathbf{W}_k$  and  $\mathbf{U}_k$  into equation (16). This approach offers two main benefits. First, the dimensions of  $\mathbf{W}_k$  and  $\mathbf{U}_k$  are significantly smaller than  $\mathbf{V}_k$ , which reduces the network size and the search space of the solution. Second, equations (14)-(16) represent the necessary conditions for the optimal solution to problem (12) [46], meaning that optimal  $\mathbf{V}_k$  must also satisfy these equations. Therefore, incorporating equation (16) into the network specifies the solution

structure and embeds the necessary expert knowledge for beamforming [28–31]. Denoting the network output as  $\bar{\mathbf{W}}_k$  and  $\bar{\mathbf{U}}_k$ , the model driven layer is formally expressed as

$$\mathbf{V}_k = \alpha_k \mathbf{B}^{-1} \mathbf{H}_k^H \bar{\mathbf{U}}_k \bar{\mathbf{W}}_k, \quad (20)$$

where

$$\mathbf{B} = \sum_{k=1}^K \frac{\sigma_k^2}{P_T} \text{Tr}(\alpha_k \bar{\mathbf{U}}_k \bar{\mathbf{W}}_k \bar{\mathbf{U}}_k^H) \mathbf{I} + \sum_{l=1}^K \alpha_l \mathbf{H}_l^H \bar{\mathbf{U}}_l \bar{\mathbf{W}}_l \bar{\mathbf{U}}_l^H \mathbf{H}_l. \quad (21)$$

### 3.4.3 Simulation Details

We assume  $K = 6$ ,  $N_t = 64$ , and  $N_r = d = 4$ . Moreover, we adopt the DeepMIMO channel, where the system configuration is provided in Table 1. To generate different wireless environments, we divide the selected region into  $4 \text{ m} \times 4 \text{ m}$  uniform blocks. An environment is specified by a  $K$ -dimension index vector, with the  $k$ th element representing the block in which user  $k$  is located.

The backbone network, referred to as SNNBeamformingNet, consists of one 2D convolutional layer with *output channel* = 36, *kernel size* =  $3 \times 3$ , and *stride* = 1; a hidden FC layer with 3,000 spiking neurons; and an output FC layer. The output is average over the  $T = 4$  simulation time steps and reshaped into  $\bar{\mathbf{W}}_k$  and  $\bar{\mathbf{U}}_k$ . These are then fed into the model-driven layer.

**Table 1:** DeepMIMO Configuration

parameter	value	parameter	value
Scenario	O1	Carrier frequency	3.5 GHz
BS array	[8 1 8]	UE array	[2 1 2]
Antenna spacing	0.5 wavelength	Radiation pattern	Isotropic
Bandwidth	128 kHz	Number of paths	25
BS index	4	UE index	800–1200

## 3.5 OFDM Channel Estimation

We consider a single-input, single-output (SISO) communication link. In OFDM systems, the input-output relationship is described as

$$\mathbf{Y}_{[i,k]} = \mathbf{H}_{[i,k]} \mathbf{X}_{[i,k]} + \mathbf{Z}_{[i,k]}, \quad (22)$$

where  $\mathbf{H} \in \mathbb{C}^{N_c \times N_s}$  represents the overall frequency-time channel response matrix, with  $N_c$  and  $N_s$  denoting the number of sub-carriers and OFDM symbols, respectively.  $\mathbf{X}_{[i,k]}$ ,  $\mathbf{H}_{[i,k]}$ ,  $\mathbf{Y}_{[i,k]}$ , and  $\mathbf{Z}_{[i,k]}$  denote the transmitted signal, the channel response, the received signal, and the AWGN at the  $i$ th sub-carrier and the  $k$ th OFDM symbol, respectively.

### 3.5.1 LS Estimator

The goal of channel estimation is to estimate  $\mathbf{H}$  based on transmitted pilots  $\mathbf{X}_p$  and received pilots  $\mathbf{Y}_p$ . Due to limited spectral resources, the pilots are sparsely inserted into the frequency-time grid. To formalize this, we define the set of all pilot positions as  $\mathcal{P}$ , where  $\mathcal{P} \in \mathcal{M}$ , and  $\mathcal{M} \triangleq \{[i, k], i, j \in \mathbb{N}, 0 < i \leq N_c, 0 < k \leq N_s\}$  represents the indices of the entire frequency-time grid. The LS estimator is given by

$$\mathbf{H}_p^{LS} = \arg \min_{\mathbf{H}_p} \|\mathbf{Y}_p - \mathbf{H}_p\|^2 = \frac{\mathbf{Y}_p}{\mathbf{X}_p}, \quad \forall p \in \mathcal{P}. \quad (23)$$

Here, the LS estimator minimizes the squared error between the received and transmitted pilot symbols at the pilot positions. The channel coefficients at the remaining frequency-time points,  $\{\mathbf{H}_q, \forall q \in \mathcal{M} \setminus \mathcal{P}\}$ , are obtained via interpolation.

### 3.5.2 LMMSE Estimator

The LMMSE estimator offers better performance than the LS estimator but requires additional information about the second-order channel statistics and noise power. Specifically, the LMMSE estimator applies a linear filter  $\mathbf{A}_{MMSE}$  to the received pilots  $\mathbf{y}_p$ :

$$\mathbf{h}_{mmse} = \mathbf{A}_{MMSE} \mathbf{y}_p, \quad (24)$$

where  $\mathbf{y}_p$  is the stacked vector of all received pilots  $\{\mathbf{Y}_p, \forall p \in \mathcal{P}\}$ . The optimal LMMSE estimator minimizes the mean-squared error (MSE) between the actual channel vector  $\mathbf{h}$  and the estimated channel vector  $\mathbf{h}_{mmse}$ :

$$\min mse \triangleq \mathbb{E}(|\mathbf{h} - \mathbf{A}_{MMSE} \mathbf{y}_p|^2), \quad (25)$$

where  $\mathbf{h}$  denotes vectorized channel matrix  $\mathbf{H}$ . By examining the first-order optimality condition, the LMMSE estimator is derived as:

$$\mathbf{A}_{MMSE} = \mathbf{R}_{\mathbf{h}, \mathbf{h}_p} (\mathbf{R}_{\mathbf{h}_p, \mathbf{h}_p} + \sigma^2 \mathbf{I})^{-1}, \quad (26)$$

where  $\mathbf{R}_{\mathbf{h}, \mathbf{h}_p} \triangleq \mathbb{E}(\mathbf{h} \mathbf{h}_p^T)$  denotes the correlation matrix between the channel response of the entire grid and the channel response at pilot positions, with  $\mathbf{h}_p$  representing the stacked

vector of  $\{\mathbf{H}_p, \forall p \in \mathcal{P}\}$ . Similarly,  $\mathbf{R}_{\mathbf{h}_p, \mathbf{h}_p} \triangleq \mathbb{E}(\mathbf{h}_p \mathbf{h}_p^T)$  denotes the autocorrelation matrix of  $\mathbf{h}_p$ , and  $\sigma^2$  represents the variance of the noise. It is worth noting that the LMMSE estimator requires prior knowledge of the channel correlation matrices, which is often impractical and therefore not included in benchmark evaluations.

### 3.5.3 Simulation Details

We assume that each OFDM frequency-time grid consists of  $N_s = 72$  subcarriers and  $N_t = 14$  OFDM symbols. The number of pilots is set to 48 and pilots are inserted into the channel grid following the way of [34]. We adopt the WINNER channel model for generating OFDM symbols and the configurations are provided in Table. 2. In our simulation, each wireless environment corresponds to a specific scenario, which are as follows: {A1 (indoor small office)-LOS, A2 (Indoor to outdoor)-NLOS, B2 (Bad urban micro-cell)-NLOS, C1 (Urban macro-cell)-NLOS, C2 (Urban macro-cell)-NLOS, C3 (Bad urban macro-cell)-NLOS, C4 (Outdoor to indoor (urban) macro-cell)-NLOS, D1 (Rural macro-cell)-LOS}. For each environment, we generate 9,000 samples for training and 1,000 samples for testing.

**Table 2:** WINNER Channel Configuration

parameter	value	parameter	value
Center frequency	5.25 GHz	Bandwidth	5 MHz–20 MHz
BS location	(150 m, 150 m, 32 m)	UE location	(110 m, 120 m, 1.5 m)
UE speed (each axis)	-0.5 m/s–0.5 m/s	Path loss	Yes
Shadow fading	Yes	Uniform sampling	No

For the backbone network, we adopt a similar architecture to ReEsNet [35]. However, we introduce two major modifications. First, the transposed convolutional layer used in ReEsNet for upsampling is replaced with a FC layer to enhance learning capacity. Second, a residual connection layer  $\mathbf{y} = \mathbf{A}\mathbf{h}_p$  is added to directly connect the input pilots with the output estimated channel. This residual connection compensates for the information loss caused by converting the real-valued channel response into spikes. It can also be interpreted as an approximation of the LMMSE estimator.

## 4 Conclusion

We proposed a neuromorphic continuous learning framework for wireless communications, named SpikACom. The framework enables two-level control on the backbone SNN. The first level of control relies on a hyper-net, which outputs modulation signals for controlling the

spiking neurons based on the distance between different channel distributions. The second level controls the synaptic weights, where a low-complexity regularization method called SRC is developed to evaluate the importance of synaptic weights. We conducted extensive experiments on representative wireless communication tasks, including task-oriented semantic communication, multi-user MIMO beamforming, and OFDM channel estimation. The simulation results demonstrated that our proposed framework could significantly alleviate catastrophic forgetting at a relatively low computational complexity and memory cost. Moreover, our network design also showcases the power of combining domain knowledge into the design of SNN modules. A comparison with conventional ANN architecture shows that SNNs could achieve performance very close to that of floating-point operation-based ANNs but with much reduced energy cost. Our work demonstrates the capability of SNNs in handling complex, large-scale wireless signal processing tasks, highlighting their potential to deliver efficient and scalable solutions for future wireless communication systems.

The authors also want to point out some limitations and future directions of this work:

1. **Theoretical Ground:** Traditional wireless communications are developed based on physical models and the algorithms are designed using statistical and/or optimization tools, which have provable performance bounds. However, for neuromorphic computing, the entire system is trained in an end-to-end manner using gradient descent, which is a black-box approach. In wireless communication, reliability is a crucial performance indicator. It is imperative to develop theoretical tools to analyse the performance of SNN-based wireless communication algorithms.
2. **Neuromorphic Hardware:** Currently, the prevailing computing architectures for deep learning are GPUs or TPUs, which are primarily designed for accelerating floating-point operation-based ANNs. However, SNNs exhibit many distinct features compared to ANNs. To fully exploit the power of SNNs, it is necessary to design neuromorphic hardware systems that are more suitable for emulating spiking neuron models. Moreover, for wireless communication, the design of neuromorphic hardware can be further customized to maximize its efficiency and efficacy.
3. **Efficient Training:** Despite the high energy efficiency of SNNs during the inference stage, training SNNs can be expensive due to their discontinuous nature. The mainstream training algorithm, BPTT, requires unrolling the SNN across the time dimension, which incurs high memory and computational costs. Therefore, introducing bio-inspired low complexity training algorithms, such as Spiking Time-Dependent Plasticity (STDP) [47], and combining them with existing gradient descent-based algorithms, can be highly beneficial.

4. **Privacy Issues:** Privacy is a general issue for data-driven learning-based algorithms, and SNNs are no exception. In wireless communications, Channel State Information (CSI) (and possibly transmitted data) is required to train neural networks, which may contain sensitive information about users. Therefore, designing privacy-preserving mechanisms for the training and updating of SNNs is a vital area for future study, which will promote broader application of SNNs in wireless communications.
5. **Standardization:** When deploying SNNs in the real world, different companies have their own trained models. Without a standardized framework, these systems may not be compatible with one another. Standardization ensures that SNN models developed by different entities can effectively communicate and operate together, facilitating a more seamless integration into existing wireless communication infrastructures. In one word, promoting the application of SNNs in wireless communication requires the collective effort of the entire ICT industry, which, the authors believe, will eventually help us build a smarter and greener information era.

## Data Availability

The DVS128 Gesture dataset [24] is available at:

<https://ibm.ent.box.com/s/3hiq58ww1pbbjrinh367ykfdf60xsfm8/folder/50167556794>.

The DeepMIMO dataset [48] is available at: <https://www.deepmimo.net/>.

The WINNER II channel model [49] is available at Matlab Communications Toolbox.

## Code Availability

The code is available at: <https://github.com/y15922/SpikACom>.

## Appendix A Generalization Bounds under EMD

Continuous learning essentially involves the ability to adapt across different data distributions. Therefore, we investigate the domain generalization bounds to get theoretical insights into our algorithms. Without loss of generality, we analyse the generalization bound for learning in two domains. A general form of this domain generalization bound can be expressed as follows:

$$R_P(h, f) \leq R_Q(h, f) + \Delta(Q, P), \quad (\text{A1})$$

where  $R_P(h, f) \triangleq \mathbb{E}_{x \sim P}[L(h(x), f(x))]$  is the risk on target domain  $P$ ,  $h$  is the hypothesis,  $f$  is the true labelling function, and  $L$  is the loss function. Likewise,  $R_Q(h, f)$  denotes the risk on source domain  $Q$ . Term  $\Delta(Q, P)$  represents a divergence measure between  $Q$  and  $P$ . In this work, we employ the Earth Mover's Distance (EMD) as the distance measure. For distributions  $Q$  and  $P$ , the EMD is defined by

$$\text{EMD}(Q, P) = \inf_{\gamma \in \Gamma(Q, P)} \int_{X \times Y} \|x - y\| d\gamma(x, y), \quad (\text{A2})$$

where  $\Gamma(Q, P)$  denotes the set of all joint distributions whose marginals are  $Q$  and  $P$ . Under EMD, the domain generalization bound can be written explicitly as follows:

**Lemma 1.** *Assume the loss function  $L$  is  $M$ -Lipschitz continuous and that  $h$  and  $f$  are  $B_h$ - and  $B_f$ -Lipschitz continuous, respectively. Then, the following bound holds:*

$$R_P(h, f) - R_Q(h, f) \leq G \cdot \text{EMD}(Q, P), \quad (\text{A3})$$

where  $G = 2M \cdot \max(B_h, B_f)$ .

*Proof.* Define  $g(x) \triangleq L(h(x), f(x))$ . Then we have

$$|g(x_1) - g(x_2)| = |L(h(x_1), f(x_1)) - L(h(x_2), f(x_2))| \quad (\text{A4a})$$

$$\leq M \sqrt{\|h(x_1) - h(x_2)\|^2 + \|f(x_1) - f(x_2)\|^2} \quad (\text{A4b})$$

$$\leq M \left( \|h(x_1) - h(x_2)\| + \|f(x_1) - f(x_2)\| \right) \quad (\text{A4c})$$

$$\leq MB_h \|x_1 - x_2\| + MB_f \|x_1 - x_2\| \quad (\text{A4d})$$

$$\leq G \|x_1 - x_2\|, \quad (\text{A4e})$$

where the first inequality applies the Lipschitz continuity of  $L$ , the second inequality applies the triangle inequality, and the third inequality applies the Lipschitz continuity of  $h$  and  $f$ . Hence,  $g(x)$  is  $G$ -Lipschitz continuous. Next,

$$R_Q(h, f) - R_P(h, f) = \mathbb{E}_{x \sim Q}[L(h(x), f(x))] - \mathbb{E}_{x \sim P}[L(h(x), f(x))] \quad (\text{A5a})$$

$$= \mathbb{E}_{x \sim Q}[g(x)] - \mathbb{E}_{x \sim P}[g(x)] \quad (\text{A5b})$$

$$\leq \sup_{\|\phi\|_L \leq G} \left( \mathbb{E}_{x \sim Q}[\phi(x)] - \mathbb{E}_{x \sim P}[\phi(x)] \right) \quad (\text{A5c})$$

$$= G \cdot \text{EMD}(Q, P), \quad (\text{A5d})$$

where the last equality uses the Kantorovich–Rubinstein duality [40]. This completes the proof.  $\square$

The following theorem quantifies how much  $R_P(h, f)$  may deviate from the performance achieved by training directly on the target distribution  $P$ .

**Theorem 1.** *Let  $h_Q^* \in \arg \min_{h \in \mathcal{H}} R_Q(h, f)$  and  $h_P^* \in \arg \min_{h \in \mathcal{H}} R_P(h, f)$ . Assume the assumptions of Lemma 1 hold and that  $L$  is symmetric and satisfies the triangle inequality. Then we have*

$$R_P(h, f) \leq R_P(h_P^*, f) + R_Q(h, h_Q^*) + G \cdot \text{EMD}(Q, P) + R_P(h_Q^*, h_P^*). \quad (\text{A6})$$

*Proof.* By the triangle inequality and Lemma 1, we obtain

$$R_P(h, f) \leq R_P(h, h_Q^*) + R_P(h_Q^*, h_P^*) + R_P(h_P^*, f), \quad (\text{A7a})$$

$$\leq R_Q(h, h_Q^*) + G \cdot \text{EMD}(Q, P) + R_P(h_Q^*, h_P^*) + R_P(h_P^*, f), \quad (\text{A7b})$$

where the first inequality follows from the triangle inequality and the second follows from Lemma 1. This completes the proof.  $\square$

The above theorem is a direct application of Theorem 8 in [50], where the discrepancy distance is replaced by the EMD. Note that  $R_Q(h, h_Q^*)$  is typically small because the hypothesis  $h$  is trained on source distribution  $Q$ , resulting in performance close to that of optimal hypothesis  $h_Q^*$ . Moreover, it is reasonable to assume that the average loss between the best in-class hypotheses,  $L_P(h_Q^*, h_P^*)$ , correlates with the distributional distance  $\text{EMD}(Q, P)$  [50]. Consequently, Theorem 1 indicates that the generalization error is primarily bounded by  $\text{EMD}(Q, P)$ . Therefore, when the two distributions  $P$  and  $Q$  are sufficiently similar, the model trained on distribution  $P$  can be applied to distribution  $Q$ , without the need for further adaption.

Recall that our SpikACom framework can intelligently control the spiking neurons of the backbone network based on distributional distances. For two similar distributions, the hypernet will activate a similar subset of spiking neurons, effectively facilitating knowledge sharing. Therefore, our algorithm is in line with the above theoretical result, which reduces the need for extensive retraining across similar domain and significantly improves efficiency.

The following theorem provides a lower bound on the generalization error but relies on more stringent assumptions.

**Assumption 1.** Hypothesis  $h_Q$  trained on the source domain satisfies

$$-\frac{1}{K} \ln q(x) - \delta \leq L(h_Q(x), f(x)) - L(h_Q^*(x), f(x)) \leq -\frac{1}{K} \ln q(x) + \delta, \quad (\text{A8})$$

where  $K$  and  $\delta$  are constants.

**Assumption 2.**

$$\text{EMD}(Q, P) \leq \sqrt{\frac{2 \text{KL}(Q \| P)}{\rho}}, \quad (\text{A9})$$

where  $\rho$  is a constant.

**Remark 1.** Assumption 1 reflects a natural phenomenon: when a hypothesis  $h_Q$  is trained on samples drawn from source distribution  $Q$ , it should be close to the optimal hypothesis  $h_Q^*$ . Furthermore, for regions of higher density  $q(x)$ , there is a greater likelihood of sampling points in those areas during training, which improves performance locally. Hence, we assume that  $L(h_Q(x), f(x)) - L(h_Q^*(x), f(x))$  is proportional to the data density  $-\ln q(x)$  and their absolute difference is bounded by  $\delta$ .

Assumption 2 states that the EMD is bounded above by the square root of the KL divergence scaled by some constant. In general, one might expect EMD to be positively related to the KL divergence since both measure distance between distributions. However, because the KL divergence is not a true distance, certain extreme cases (e.g., two sharply peaked Gaussian distributions with different means) may invalidate this assumption. We stress that such cases rarely arise in practice. Hence, to streamline our analysis, we adopt this inequality as an assumption. Notably, the same inequality also arises as a sufficient condition for the Talagrand inequality [51].

**Lemma 2.** Assuming that Assumption 1, Assumption 2, and the assumptions of Lemma 1 hold, we have

$$\begin{aligned} R_P(h_Q, f) - R_Q(h_Q, f) &\geq R_P(h_Q^*, f) - R_Q(h_Q^*, f) - 2\delta + \frac{1}{K}(H(P) - H(Q)) \\ &\quad + \frac{\rho}{2K} \text{EMD}(Q, P)^2. \end{aligned} \quad (\text{A10})$$

*Proof.*

$$R_P(h_Q, f) - R_Q(h_Q, f) \quad (\text{A11a})$$

$$= \int L(h_Q(x), f(x)) p(x) dx - \int L(h_Q(x), f(x)) q(x) dx \quad (\text{A11b})$$

$$\geq \int [L(h_Q^*(x), f(x)) - \frac{\ln q(x)}{K} - \delta] p(x) dx - \int [L(h_Q^*(x), f(x)) - \frac{\ln q(x)}{K} + \delta] q(x) dx \quad (\text{A11c})$$

$$= R_P(h_Q^*, f) - \frac{1}{K} \int \ln q(x) p(x) dx - 2\delta - R_Q(h_Q^*, f) - \frac{1}{K} H(Q) \quad (\text{A11d})$$

$$= R_P(h_Q^*, f) - R_Q(h_Q^*, f) - 2\delta + \frac{1}{K} (H(P) - H(Q) + \text{KL}(P\|Q)) \quad (\text{A11e})$$

$$\geq R_P(h_Q^*, f) - R_Q(h_Q^*, f) - 2\delta + \frac{1}{K} (H(P) - H(Q)) + \frac{\rho}{2K} \text{EMD}(Q, P)^2, \quad (\text{A11f})$$

where (A11c) applies Assumption 1, and (A11e) follows from the definition of the KL divergence. The final inequality applies Assumption 2.  $\square$

The following theorem states a lower bound on how much  $R_P(h_Q, f)$  can deviate from  $R_P(h_P^*, f)$ .

**Theorem 2.** *Assuming that the conditions of Lemma 2 hold, we have the following lower bound on the generalization error:*

$$R_P(h_Q, f) - R_P(h_P^*, f) \geq \frac{\rho}{2K} \text{EMD}(Q, P)^2 + \frac{1}{K} (H(P) - H(Q)) - 2\delta. \quad (\text{A12})$$

*Proof.*

$$R_P(h_Q, f) - R_P(h_P^*, f) = R_P(h_Q, f) - R_Q(h_Q, f) + R_Q(h_Q, f) - R_P(h_P^*, f) \quad (\text{A13a})$$

$$\geq R_P(h_Q^*, f) - R_Q(h_Q^*, f) - 2\delta + \frac{1}{K} (H(P) - H(Q)) + \frac{\rho}{2K} \text{EMD}(Q, P)^2$$

$$+ R_Q(h_Q, f) - R_P(h_P^*, f) \quad (\text{A13b})$$

$$= R_P(h_Q^*, f) - R_P(h_P^*, f) + R_Q(h_Q, f) - R_Q(h_Q^*, f) - 2\delta + \frac{1}{K} (H(P) - H(Q))$$

$$+ \frac{\rho}{2K} \text{EMD}(Q, P)^2 \quad (\text{A13c})$$

$$\geq \frac{\rho}{2K} \text{EMD}(Q, P)^2 + \frac{1}{K} (H(P) - H(Q)) - 2\delta, \quad (\text{A13d})$$

where (A13b) applies Lemma 2 and the last inequality follows from  $R_P(h_Q^*, f) - R_P(h_P^*, f) \geq 0$  and  $R_Q(h_Q, f) - R_Q(h_Q^*, f) \geq 0$ . This completes the proof.  $\square$

Theorem 2 establishes that the generalization error is lower bounded by three terms. The first term is the square of the EMD. The second term captures the difference between the target distribution's entropy and the source domain's entropy. This suggests that training on a more diverse data distribution can enhance generalization ability. However, in our continuous learning setup, the entropies of different wireless environments are typically similar, rendering this term negligible. The third term measures how strictly Assumption 1 holds,

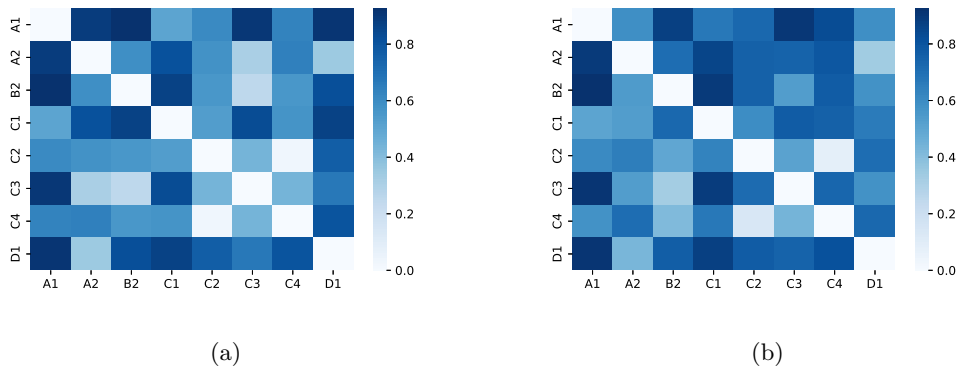


**Fig. A1:** Comparison between the EMD and the generalization error  $R_P(h, f) - R_P(h_P^*, f)$  in OFDM channel estimation task. (a) The EMDs between the eight WINNERII channel model scenarios. (b) The generalization errors between the eight channel distributions, which are normalized for better visualization.

which we consider to be small. Therefore, the principal factor contributing to the lower generalization bound is the EMD term.

Since the EMD is symmetric, two distributions with a large EMD will yield high generalization errors in both directions—namely, from  $P$  to  $Q$  and from  $Q$  to  $P$ . This observation implies that, when only data from the current environment is available, a single hypothesis  $h$  cannot concurrently achieve optimal performance on both distributions if they differ significantly. Regularization-based methods, such as EWC, fall into this category and thus perform poorly when the distance between distributions is large. Theorem 2 therefore underscores the necessity of introducing new plasticity in continuous learning—when the new distribution differs significantly from all previously learned ones. Our SpikACom embodies this principle by activating a different subset of spiking neurons upon encountering a distinctly new environment. Hence, it can simultaneously achieves satisfactory performance on both current and previous environments.

We validate the above theorems using experimental results. Fig. A1 compares the EMD and the generalization error for the OFDM channel estimation task, where the EMD is computed via our proposed FCD approach for reduced computational cost. As shown, the EMD is positively related to the generalization error.

## Appendix B Generalization between Inter-Tasks Distributions

As pointed out in [52], a desirable solution in the context of continual learning requires inter-task generalization to accommodate distributional shifts. In mainstream machine learning, deriving such relationships is challenging due to the absence of a unified physical framework. However, wireless communications benefit from precise and well-understood physical models that accurately describe how signals propagate through different environments. The consistent physical models provide a stable foundation upon which generalizable algorithms can build, ensuring that learning remains robust and adaptable across different scenarios.

As an illustrative example, we consider task-oriented semantic communication. Specifically, consider an  $L$ -tap multi-path channel model. Denote the transmitted spikes by  $x$ , the channel by  $h$ , and the received signal (without noise) by

$$y[k] = \sum_{l=1}^L h[l]x[k-l]. \quad (\text{B14})$$

Since the primary focus is on the distributional shifts of the channels, we assume that  $x[k]$ s are independent with each other. Moreover, we adopt the widely used assumption that the instantaneous channel response of each path follows a complex Gaussian distribution  $h[l] \sim \mathcal{CN}\{0, g_l\}$  [53], where  $g_l$  is the average gain of the  $l$ -th path. Under a rich scattering environment (i.e.,  $L \rightarrow \infty$ ), the Central Limit Theorem [54] implies that

$$y[k] \sim \mathcal{CN}(0, p_x G), \quad (\text{B15})$$

where  $p_x = E(x)$  denotes the average firing probability of the transmitting spiking neurons and  $G \triangleq \sum_l^L g_l^2$  denotes the overall path gain. Hence, for two channel distributions  $\mathcal{H}_1$  and  $\mathcal{H}_2$  whose total path gains are  $G_1$  and  $G_2$ , respectively, the EMD between the received signals  $y_1$  and  $y_2$  can be computed as

$$\text{EMD}(y_1, y_2) = p_x (\sqrt{G_1} - \sqrt{G_2})^2. \quad (\text{B16})$$

Since we want a channel distance measure independent of the input, we divide it by  $p_x$  and define

$$\text{EMD}(\mathcal{H}_1, \mathcal{H}_2) = (\sqrt{G_1} - \sqrt{G_2})^2. \quad (\text{B17})$$

By leveraging domain knowledge, we derive a concise expression for the EMD between different multipath channels. This enables straightforward generation of diverse channel environments for hypernet training. However, since the goal of the hypernet is to distinguish

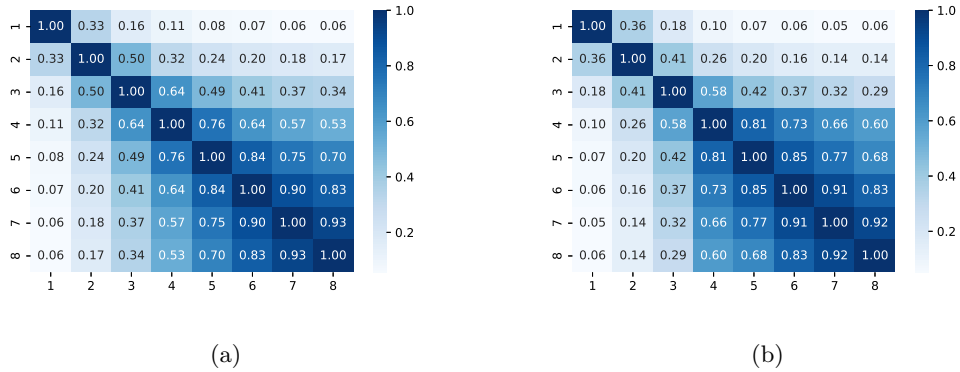


**Fig. B2:** Generalization performance of the hypernet to unseen environments. (a) The EMD between the eight wireless environments. (b) The cosine distance between the hypernet gates. The hypernet is trained on 60 channel distributions and tested on 8 unseen environments.

among environments, it actually requires relatively few samples for adaptation. In our experiment, we generate only 60 channel distributions to train the hypernet and test it on 8 unseen environments. Fig. B2 presents the numerical results. Notably, the cosine distance of the hyper gate closely aligns with the EMD, indicating that the hypernet generalizes effectively across different channel environments.

In general scenarios, the channel propagation environment may be complex, necessitating data-driven methods to distinguish different environments such as our proposed FCD. Under such a case, collecting a few amount of channel samples would be necessary for hypernet training. Even then, our SpikACom retains several key advantages. First, fundamental physical models (e.g., multipath propagation) remain valid, which provides a foundation for generalization across diverse channel distributions. This contrasts with fields such as computer vision or natural language processing, where no common physical model exists. Second, SpikACom decomposes the system into a hypernet for capturing the relationships among different wireless environments, and a backbone network for executing tasks. Thus, the burden of generalization is concentrated on the hypernet, making adaptation simpler since it only needs to identify the environments, as demonstrated by Fig. B2. Finally, this decomposition increases the flexibility of the wireless communication system. Since the hypernet is task-agnostic, it can be simultaneously applied to multiple wireless communication tasks, thus enhancing overall efficiency.

**Table C1:** Permutation Orders of Wireless Environments

Time Index	1	2	3	4	5	6	7	8
Order 1 (↓)	0 dB	-4 dB	-8 dB	-12 dB	-16 dB	-20 dB	-24 dB	-28 dB
Order 2 (↑)	-28 dB	-24 dB	-20 dB	-16 dB	-12 dB	-8 dB	-4 dB	0 dB
Order 3	-12 dB	-24 dB	-8 dB	-28 dB	0 dB	-20 dB	-4 dB	-16 dB
Order 4	-20 dB	-24 dB	-16 dB	-12 dB	-8 dB	-4 dB	-28 dB	0 dB
Order 5	-8 dB	-24 dB	-28 dB	-4 dB	0 dB	-16 dB	-20 dB	-12 dB
Order 6	-24 dB	-28 dB	0 dB	-8 dB	-16 dB	-12 dB	-4 dB	-20 dB
Order 7	-16 dB	-20 dB	-24 dB	-28 dB	-8 dB	-12 dB	-4 dB	0 dB

## Appendix C Impact of Permutations

We investigate the impact of permutations on our algorithm. Specifically, we validate the performance on task-oriented semantic communication task and examine seven permutations: one in ascending order of SNR, one in descending order of SNR, and five in random orders. The detailed orders of the arriving wireless environments are presented in Table C1.

Table C2 compares our proposed algorithm against three baselines, including the Random Weight (no forgetting), Sequential Training (no forgetting), and EWC baselines. The Random Weight (no forgetting) scheme initializes a new SNN with randomly assigned weights whenever a new environment arrives (at additional memory cost). Consequently, it does not suffer from catastrophic forgetting or plasticity loss. The Sequential Training (no forgetting) scheme also uses a new SNN for each environment but initializes the weights using those trained in the last environment. Therefore, both the Random Weight scheme and Sequential Training (No Forgetting) scheme serve as ideal benchmarks to examine the impact of permutation orders on performance.

From Table C2, we observe that the Random Weight approach consistently achieves an accuracy of 71.74%. This scheme is unaffected by permutations because it always uses a new SNN with randomly initialized weights for training whenever a new environment comes, which serves as an idealized baseline with full plasticity. However, the Sequential Training approach is sensitive to permutations. When environments arrive in descending order of SNR, Sequential Training achieves 77.76% accuracy, higher than random initialization. However, in ascending SNR order, its accuracy drops to 54.20%. Therefore, when the network starts training based on previously acquired knowledge (which is exactly the case in continuous learning), the order of environments will have an impact on the performance.

We conjecture the following explanation. When the network starts in a high SNR environment, semantic features are easier to distinguish due to minimal noise. As a result, the

**Table C2:** Performance Comparison Under Different Permutations

<b>Order</b>	<b>1 (↓)</b>	<b>2 (↑)</b>	<b>3</b>	<b>4</b>	<b>5</b>	<b>6</b>	<b>7</b>
Random weight (no forgetting)	71.74	71.74	71.74	71.74	71.74	71.74	71.74
Sequential (no forgetting)	77.76	54.20	75.93	65.95	75.43	67.98	70.94
Proposed	77.42	62.01	74.65	71.27	74.69	71.97	72.07
EWC	71.54	35.66	73.94	61.98	74.41	43.86	60.00
Proposed (dropped accuracy)	0.43	1.61	0.43	0.88	0.10	1.65	0.56

encoder–decoder pair learns a robust representation for the transmission and recognition of semantic feature. In subsequent low SNR environments, the previously learned representation remains beneficial, requiring the system only to develop additional denoising abilities. Hence, in a descending SNR scenario, Sequential Training can outperform Random Weight. However, if the network first encounters a low SNR environment, the semantic features are obscured by noise. Consequently, the decoder primarily learns to denoise the data rather than distinguish semantic features. When subsequently exposed to high SNR environments, the previously acquired denoising-centric knowledge becomes less relevant. In contrast, it potentially gets the SNN trapped in local optima and results in poorer performance than random initialization.

Our proposed method demonstrates greater robustness to permutation orders than the Sequential Training scheme. Specifically, it achieves an average accuracy of 77.42% in the descending SNR order, closely matching the Sequential Training scheme’s 77.76%. In the ascending SNR order, our method attains an average accuracy of 62.01%, outperforming the Sequential Training scheme’s 54.20%. This robustness is attributed to our algorithm’s intelligent introduction of an appropriate amount of new plasticity, enabling the network to escape local optima and achieve superior performance compared to Sequential Training. In other random-order scenarios, our proposed algorithm consistently achieves similar or better performance than the Random Weight scheme and demonstrates greater robustness than Sequential Training. On the other hand, EWC exhibits the highest sensitivity to permutation orders, with accuracy fluctuating significantly across different orders. This sensitivity arises because EWC imposes regularization on the training weights, constraining them to remain close to the parameters learned in the initial environments. As a result, if the SNN starts in a low SNR environment, the weights will be significantly restricted, leading to poor performance in subsequent environments. Finally, the average dropped accuracy of our proposed algorithm is within 2%. This minimal drop underscores the algorithm’s robustness to permutation in terms of stability.

## Appendix D Extension to Convolutional Layers

In the previous sections, we introduced our proposed method, SpikACom, based on fully connected (FC) layers. However, convolutional layers are also widely used in SNNs. This section explains how to adapt SpikACom for use in spiking convolutional layers.

### D.1 Hypernet

The hypernet outputs a binary gate to control the backbone network based on the distributional distance of different wireless environments. For fully connected (FC) layers, the binary gate directly regulates the activation of output spiking neurons. This mechanism can effectively mitigate inter-task interference. As an illustrative example, consider an FC layer with a weight matrix  $\mathbf{W}$ , an input spike vector  $\mathbf{s}$ , and a hypernet gate  $\mathbf{g}$ . The output can be expressed as

$$\mathbf{y} = \mathbf{g} \circ f(\mathbf{W}\mathbf{s}), \quad (\text{D18})$$

where  $f$  denotes the neuron model, which is applied element-wise. For two environments  $\mathcal{H}_1$  and  $\mathcal{H}_2$ , the inner product of the gradients with respect to  $\mathbf{W}$  is given by

$$\begin{aligned} \left\langle \frac{\partial L_1}{\partial \mathbf{W}}, \frac{\partial L_2}{\partial \mathbf{W}} \right\rangle &= \left\langle \left[ \frac{\partial L_1}{\partial \mathbf{y}_1} \circ \mathbf{g}_1 \circ f'(\mathbf{W}\mathbf{s}_1) \right] \mathbf{s}_1^T, \left[ \frac{\partial L_2}{\partial \mathbf{y}_2} \circ \mathbf{g}_2 \circ f'(\mathbf{W}\mathbf{s}_2) \right] \mathbf{s}_2^T \right\rangle \\ &= \text{Tr}(\mathbf{a}_1^T \mathbf{a}_2 \mathbf{s}_1^T \mathbf{s}_2), \end{aligned} \quad (\text{D19})$$

where  $\mathbf{a}_1 = \frac{\partial L_1}{\partial \mathbf{y}_1} \circ \mathbf{g}_1 \circ f'(\mathbf{W}\mathbf{s}_1)$  and  $\mathbf{a}_2 = \frac{\partial L_2}{\partial \mathbf{y}_2} \circ \mathbf{g}_2 \circ f'(\mathbf{W}\mathbf{s}_2)$ . Therefore, for two environments with orthogonal gates ( $\langle \mathbf{g}_1, \mathbf{g}_2 \rangle = 0$ ), we have  $\mathbf{a}_1^T \mathbf{a}_2 = 0$ , which leads to

$$\left\langle \frac{\partial L_1}{\partial \mathbf{W}}, \frac{\partial L_2}{\partial \mathbf{W}} \right\rangle = 0.$$

This indicates that there is no interference between the two environments if the gates are orthogonal.

However, in convolutional networks,  $\langle \mathbf{g}_1, \mathbf{g}_2 \rangle = 0$  does not necessarily result in  $\langle \frac{\partial L_1}{\partial \mathbf{W}}, \frac{\partial L_2}{\partial \mathbf{W}} \rangle = 0$ . This is because in convolutional layers, all elements in an output feature map share a single convolutional kernel. Consequently, during the back-propagation stage, gradients can still propagate through the same convolutional kernel, leading to interference even if two environments activate orthogonal parts of the feature map.

To address this issue, we utilize the hypernet gate to control the on-off of output channels, as illustrated in Fig. D3. By gating at the channel level, orthogonal hypernet gates ensure that the learning parameter spaces of the backbone SNN are orthogonal. This approach effectively prevents unnecessary inter-task interference, similar to the mechanism used in FC layers.

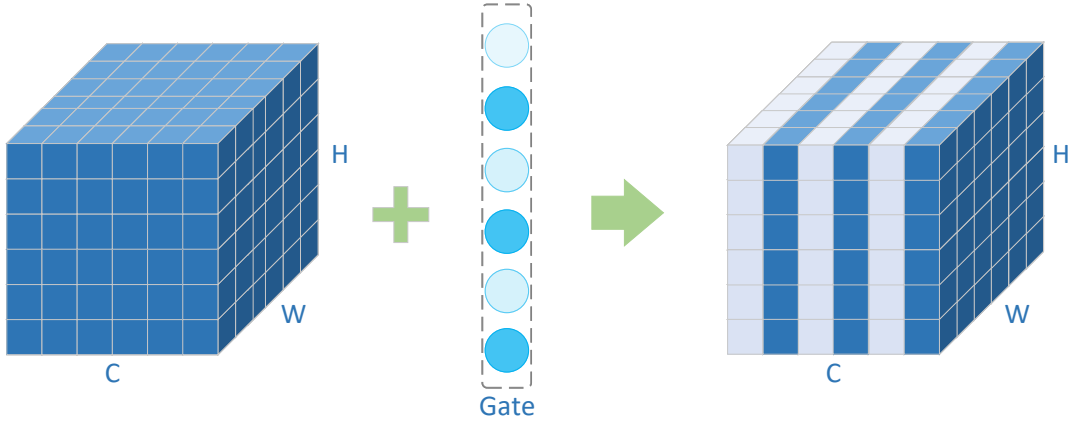


**Fig. D3:** An illustration of how the output gate of hypernet modulates the spiking convolutional layers.

## D.2 SRC for Spiking CNNs

Recall that in FC layers, our proposed SRC imposes a regularization term on the synaptic weights, defined as

$$\mathcal{L}_{\text{reg}}^F = \sum_l \Omega_l^F \circ \mathbf{W}^F, \quad (\text{D20})$$

where  $\mathbf{W}^F$  denotes the synaptic weights of the FC layer and  $\Omega_l^F \triangleq \mathbf{u}_l^F \mathbf{v}_l^{F\top}$  denotes the importance of the synaptic weights to the  $l$ -th environment. Here,  $\mathbf{u}_l^F$  and  $\mathbf{v}_l^F$  denote the spiking rate vectors of the input and output layers, respectively. For simplicity, the subscript  $l$  is omitted in the following discussions.

The core idea of SRC is to use the level of neuron activity to represent the importance of the synaptic weights. In FC layers, synaptic weight  $w_{i,j}^F$  connects input neuron  $i$  to output neuron  $j$ , and its regularization weight is simply given by  $u_i \times v_j$ . Then, we extend the idea to convolutional layers. Consider a convolutional layer with  $I$  input channels,  $J$  output channels, a kernel size of  $K \times K$ , an output feature map size of  $H \times W$ , and a stride of 1. Given the definition of convolution, the convolutional kernel  $\mathbf{W}_{i,j}^C \in \mathbb{R}^{K \times K}$  convolves across the entire  $i$ -th input feature map to produce the  $j$ -th output feature map. Therefore, we define the regularization weight for  $\mathbf{W}_{i,j}^C$  as  $u_i^C \times v_j^C$ , where  $u_i^C$  and  $v_j^C$  represent the summation of the spiking rates of the  $i$ -th input channel and the  $j$ -th output channel, respectively.

In short, denoting the stacked vectors of  $u_i^C$  and  $v_j^C$  as  $\mathbf{u}^C$  and  $\mathbf{v}^C$ , respectively, the SRC regularization for the convolutional layer is expressed as

$$\mathcal{L}_{\text{reg}}^C = \Omega^C \circ \mathbf{W}^C, \quad (\text{D21})$$

where

$$\boldsymbol{\Omega}^C \triangleq \mathbf{u}^C \otimes \mathbf{v}^C \otimes \mathbf{1} \otimes \mathbf{1},$$

and  $\otimes$  denotes the tensor product.

## Appendix E Energy Consumption Model

We calculate the energy consumption of SNNs based on the number of floating-point operations (FLOPs). For a spiking convolutional layer with  $C_{in}$  input channels,  $C_{out}$  output channels, a kernel size of  $K \times K$ , and an output size of  $H_{out} \times W_{out}$ , the FLOPs can be expressed as

$$FLOP = H_{out} \times W_{out} \times C_{out} \times C_{in} \times K^2 \times p. \quad (\text{E22})$$

where  $p$  represents the average spiking rate of the neurons in the input channels. Compared with ANNs, SNNs exhibit two key differences in energy consumption. First, the energy consumption of SNN is related to the firing probability of spiking neurons, which means lower neural activity will lead to reduced energy usage. In ANNs, however,  $p$  is consistently equal to 1. Second, in most cases, the input to SNNs consists of binary spikes, allowing the energy demanding multiply-and-accumulate (MAC) operations to be simplified to accumulate (AC) operations. In contrast, MAC operations are unavoidable in ANNs. To quantify the energy consumption, we employ the energy model on a 45 nm CMOS chip [11, 55], which specifies  $E_{mac} = 3.2$  pJ and  $E_{ac} = 0.1$  pJ. Therefore, the total energy consumption of SNNs is given by

$$E_{snn} = \sum_{l \in \mathcal{S}} E_{ac} \times FLOP_l \times T + \sum_{l \in \mathcal{S}'} E_{mac} \times FLOP_l. \quad (\text{E23})$$

where  $\mathcal{S}$  represents the set of SNN layers that receive spike inputs and  $\mathcal{S}'$  denotes the set of SNN layers that involves MAC operations, such as the input layer.

In our beamforming experiment, the model-driven layer involves matrix inversion operations. We utilize the model presented in [56] to calculate the FLOPs required for matrix inversion. Specifically, for square matrix  $\mathbf{A}$  of size  $n \times n$ , the FLOPs required to compute  $\mathbf{A}^{-1}$  is approximately  $\frac{1}{2}n^3$ . Hence, the energy required for matrix inversion is given by

$$E_{inv} = E_{mac} \times \frac{1}{2}n^3. \quad (\text{E24})$$

## References

- [1] Han, S., Bian, S. *et al.* Energy-efficient 5G for a greener future. *Nat. Electron.* **3**, 182–184 (2020).

- [2] Smarter 2030: Ict solutions for 21st century challenges (2015). Global e-Sustainability Initiative [https://smarter2030.gesi.org/downloads/Full\\_report.pdf](https://smarter2030.gesi.org/downloads/Full_report.pdf).
- [3] The enablement effect: The impact of mobile communications technologies on carbon emission reductions (2020). GSMA [https://smarter2030.gesi.org/downloads/Full\\_report.pdf](https://smarter2030.gesi.org/downloads/Full_report.pdf).
- [4] Green 5g: Building a sustainable world (2020). Huawei Technologies Co., Ltd., <https://www.huawei.com/en/public-policy/green-5g-building-a-sustainable-world>.
- [5] Katsaros, G. N., Tafazolli, R. & Nikitopoulos, K. *On the power consumption of massive-MIMO, 5G new radio with software-based PHY processing*, In Proc. 2022 IEEE Globecom Workshops (GC Wkshps), 765–770 (IEEE, 2022).
- [6] Zhang, C., Patras, P. & Haddadi, H. Deep learning in mobile and wireless networking: A survey. *IEEE Commun. Surv. Tutor.* **21**, 2224–2287 (2019).
- [7] Tong, W. & Li, G. Y. Nine challenges in artificial intelligence and wireless communications for 6G. *IEEE Wireless Commun.* **29**, 140–145 (2022).
- [8] Mehonic, A. & Kenyon, A. J. Brain-inspired computing needs a master plan. *Nature* **604**, 255–260 (2022).
- [9] Borsos, T., Condoluci, M., Daoutis, M., Haga, P. & Veres, A. *Resilience analysis of distributed wireless spiking neural networks*, In Proc. 2022 IEEE Wireless Communications and Networking Conference (WCNC), 2375–2380 (IEEE, 2022).
- [10] Skatchkovsky, N., Jang, H. & Simeone, O. *Federated neuromorphic learning of spiking neural networks for low-power edge intelligence*, In Proc. 2020 IEEE International Conference on Acoustics, Speech, and Signal Processing (ICASSP), 8524–8528 (IEEE, 2020).
- [11] Yang, H. *et al.* Lead federated neuromorphic learning for wireless edge artificial intelligence. *Nat. commun.* **13**, 4269 (2022).
- [12] Chen, J., Skatchkovsky, N. & Simeone, O. Neuromorphic wireless cognition: Event-driven semantic communications for remote inference. *IEEE Trans. Cogn. Commun. Netw.* **9**, 252–265 (2023).

- [13] Wang, M., Li, J., Ma, M. & Fan, X. Spiking semantic communication for feature transmission with HARQ. *arXiv preprint arXiv:2310.08804* (2023).
- [14] Skatchkovsky, N., Jang, H. & Simeone, O. *End-to-end learning of neuromorphic wireless systems for low-power edge artificial intelligence*, In Proc. 2020 54th Asilomar Conference on Signals, Systems, and Computers, 166–173 (IEEE, 2020).
- [15] Chen, J., Skatchkovsky, N. & Simeone, O. Neuromorphic integrated sensing and communications. *IEEE Wireless Commun. Lett.* **12**, 476–480 (2022).
- [16] Jiang, Q. & Sha, J. The use of SNN for ultralow-power RF fingerprinting identification with attention mechanisms in VDES-SAT. *IEEE Internet Things J.* **10**, 15594–15603 (2023).
- [17] Dakic, K., Homssi, B. A., Walia, S. & Al-Hourani, A. Spiking neural networks for detecting satellite-based internet-of-things signals. *arXiv preprint arXiv:2304.03896* (2023).
- [18] Wang, L., Zhang, X., Su, H. & Zhu, J. A comprehensive survey of continual learning: Theory, method and application. *IEEE Trans. Pattern Anal. Mach. Intell.* (2024).
- [19] Liu, F., Zhao, W., Chen, Y., Wang, Z. & Dai, F. *Dynsnn: A dynamic approach to reduce redundancy in spiking neural networks*, In Proc. 2022 IEEE International Conference on Acoustics, Speech, and Signal Processing (ICASSP), 2130–2134 (IEEE, 2022).
- [20] Kirkpatrick, J. *et al.* Overcoming catastrophic forgetting in neural networks. *Proc. Natl. Acad. Sci.* **114**, 3521–3526 (2017).
- [21] Gündüz, D. *et al.* Beyond transmitting bits: Context, semantics, and task-oriented communications. *IEEE J. Sel. Areas Commun.* **41**, 5–41 (2022).
- [22] Bourtsoulatze, E., Kurka, D. B. & Gündüz, D. Deep joint source-channel coding for wireless image transmission. *IEEE Trans. Cogn. Commun. Netw.* **5**, 567–579 (2019).
- [23] Xie, H., Qin, Z., Li, G. Y. & Juang, B.-H. Deep learning enabled semantic communication systems. *IEEE Trans. Signal Process.* **69**, 2663–2675 (2021).
- [24] Amir, A. *et al.* *A low power, fully event-based gesture recognition system*, In Proc. IEEE Conference on Computer Vision and Pattern Recognition, 7243–7252 (2017).

- [25] Schuster, M. & Paliwal, K. K. Bidirectional recurrent neural networks. *IEEE Trans. Signal Process.* **45**, 2673–2681 (1997).
- [26] Hochreiter, S. & Schmidhuber, J. Long short-term memory. *Neural Comput.* **9**, 1735–1780 (1997).
- [27] Lu, L., Li, G. Y., Swindlehurst, A. L., Ashikhmin, A. & Zhang, R. An overview of massive MIMO: Benefits and challenges. *IEEE J. Sel. Top. Signal Process.* **8**, 742–758 (2014).
- [28] Xia, W. *et al.* A deep learning framework for optimization of MISO downlink beamforming. *IEEE Trans. Commun.* **68**, 1866–1880 (2019).
- [29] Zhang, M., Gao, J. & Zhong, C. A deep learning-based framework for low complexity multiuser MIMO precoding design. *IEEE Trans. Wireless Commun.* **21**, 11193–11206 (2022).
- [30] Lu, S., Zhao, S. & Shi, Q. *Learning-based massive beamforming*, In Proc. 2020 IEEE Global Communications Conference, 1–6 (IEEE, 2020).
- [31] Hu, Q. *et al.* Iterative algorithm induced deep-unfolding neural networks: Precoding design for multiuser MIMO systems. *IEEE Trans. Wireless Commun.* **20**, 1394–1410 (2020).
- [32] Ye, H., Li, G. Y. & Juang, B.-H. Power of deep learning for channel estimation and signal detection in OFDM systems. *IEEE Wireless Commun. Lett.* **7**, 114–117 (2017).
- [33] Hwang, T., Yang, C., Wu, G., Li, S. & Li, G. Y. OFDM and its wireless applications: A survey. *IEEE Trans. Vehicular Technol.* **58**, 1673–1694 (2008).
- [34] Soltani, M., Pourahmadi, V., Mirzaei, A. & Sheikhzadeh, H. Deep learning-based channel estimation. *IEEE Commun. Lett.* **23**, 652–655 (2019).
- [35] Li, L., Chen, H., Chang, H.-H. & Liu, L. Deep residual learning meets OFDM channel estimation. *IEEE Wireless Commun. Lett.* **9**, 615–618 (2019).
- [36] Fang, W. *et al.* Spikingjelly: An open-source machine learning infrastructure platform for spike-based intelligence. *Sci. Adv.* **9**, eadi1480 (2023).

- [37] Neftci, E. O., Mostafa, H. & Zenke, F. Surrogate gradient learning in spiking neural networks: Bringing the power of gradient-based optimization to spiking neural networks. *IEEE Signal Process. Mag.* **36**, 51–63 (2019).
- [38] Zhao, R. *et al.* A framework for the general design and computation of hybrid neural networks. *Nat. Commun.* **13**, 3427 (2022).
- [39] Mallya, A., Davis, D. & Lazebnik, S. *Piggyback: Adapting a single network to multiple tasks by learning to mask weights*, In Proc. European Conference on Computer Vision (ECCV), 67–82 (2018).
- [40] Arjovsky, M., Chintala, S. & Bottou, L. *Wasserstein generative adversarial networks*, In Proc. International Conference on Machine Learning, 214–223 (PMLR, 2017).
- [41] Heusel, M., Ramsauer, H., Unterthiner, T., Nessler, B. & Hochreiter, S. GANs trained by a two time-scale update rule converge to a local Nash equilibrium **30** (2017).
- [42] Wen, C.-K., Shih, W.-T. & Jin, S. Deep learning for massive MIMO CSI feedback. *IEEE Wireless Commun. Lett.* **7**, 748–751 (2018).
- [43] Szegedy, C., Vanhoucke, V., Ioffe, S., Shlens, J. & Wojna, Z. *Rethinking the Inception architecture for computer vision*, In Proc. IEEE Conference on Computer Vision and Pattern Recognition, 2818–2826 (2016).
- [44] Fang, W. *et al.* *Incorporating learnable membrane time constant to enhance learning of spiking neural networks*, In Proc. IEEE/CVF International Conference on Computer Vision, 2661–2671 (2021).
- [45] Ye, H., Li, G. Y. & Juang, B.-H. Deep learning based end-to-end wireless communication systems without pilots. *IEEE Trans. Cogn. Commun. Netw.* **7**, 702–714 (2021).
- [46] Shi, Q., Razaviyayn, M., Luo, Z.-Q. & He, C. An iteratively weighted MMSE approach to distributed sum-utility maximization for a MIMO interfering broadcast channel. *IEEE Trans. Signal Process.* **59**, 4331–4340 (2011).
- [47] Bi, G. & Poo, M. Synaptic modifications in cultured hippocampal neurons: Dependence on spike timing, synaptic strength, and postsynaptic cell type. *Journal of neuroscience* **18**, 10464–10472 (1998).

- [48] Alkhateeb, A. Deepmimo: A generic deep learning dataset for millimeter wave and massive mimo applications. *arXiv preprint arXiv:1902.06435* (2019).
- [49] Bultitude, Y. d. J. & Rautiainen, T. Ist-4-027756 winner ii d1. 1.2 v1. 2 winner ii channel models. *NOKIA, Tech. Rep* (2007).
- [50] Mansour, Y., Mohri, M. & Rostamizadeh, A. Domain adaptation: Learning bounds and algorithms. *arXiv preprint arXiv:0902.3430* (2009).
- [51] Villani, C. *Topics in optimal transportation* (American Mathematical Soc., 2021).
- [52] Wang, L., Zhang, X., Su, H. & Zhu, J. A comprehensive survey of continual learning: Theory, method and application. *IEEE Trans. Pattern Anal. Mach. Intell.* (2024).
- [53] Ye, H., Li, G. Y. & Juang, B.-H. Deep learning based end-to-end wireless communication systems without pilots. *IEEE Trans. Cogn. Commun. Netw.* **7**, 702–714 (2021).
- [54] Billingsley, P. *Probability and measure* (John Wiley & Sons, 2017).
- [55] Horowitz, M. *1.1 computing’s energy problem (and what we can do about it)*, In Proc. 2014 IEEE International Solid-State Circuits Conference (ISSCC), 10–14 (IEEE, 2014).
- [56] Krishnamoorthy, A. & Menon, D. *Matrix inversion using Cholesky decomposition*, In Proc. 2013 Signal Processing: Algorithms, Architectures, Arrangements, and Applications (SPA), 70–72 (IEEE, 2013).